STUDY OF REDUCED ORDER MODELS FOR VORTEX-INDUCED VIBRATION AND COMPARISON WITH CFD RESULTS

BY

CHRISTOPHER WILLIAM OLENEK

THESIS

Submitted in partial fulfillment of the requirements
for the degree of Master of Science in Mechanical Engineering
in the Graduate College of the
University of Illinois at Urbana-Champaign, 2011

Urbana, Illinois

Advisors:

Professor Lawrence A. Bergman
Professor Alexander F. Vakakis

Abstract

Vortex-induced vibration (VIV) is a dynamic phenomenon that can occur when there is fluid flow past a bluff body with flexibility. Over time, VIV can cause fatigue damage, so it may be desirable to suppress these vibrations. It is important to understand how the system behaves when trying to control vibrations; a reduced order model may be an effective way to study the system dynamics. Developing a data driven model from simulation and/or experimental results can be difficult, but there are existing phenomenological models that attempt to describe VIV, several of which will be explored in this thesis. These models consist of a structural equation representing a simple sprung bluff body coupled to a wake equation representing the effects of the surrounding fluid on the oscillator; the latter is generally a nonlinear oscillator exhibiting limit cycle behavior. The coupling, structural equation, and type of nonlinearity in the wake equation vary between different models, and the effects of these differences will be explored. The parameters of these equations must be identified, and then results from these models will be compared with the results obtained from a high fidelity CFD simulation to determine the relative quality of each reduced order model. The deficiencies of each model and the effects they produce will also be explored. Finally, the most important traits of each reduced order model will be identified, and, finally, the best reduced order model, with specific parameter values, will be presented.

Acknowledgments

I want to express my gratitude to the many people who have helped me along the way toward accomplishing this goal. I'd like to thank Professor Alexander Vakakis for his support and giving me the chance to complete a thesis with a very accomplished and impressive research group. I'd also like to thank Professor Larry Bergman for his patience in helping me complete this thesis and make it the best it can be. I'd like to give a special thanks to Professor Arif Masud and Ramon Calderer who developed the CFD code that was essential to this study. I'd like to also give special thanks to Ravi Kumar; his constant willingness to help me and guide me in the right direction when things became difficult was a necessity, and without him, this study would not have been possible. In addition, I'd like to express my gratitude towards every member of the LNDVL for being an exciting and dynamic research group that I am proud to be a part of. Finally, I'd like to thank my family, friends, and girlfriend for their support during this time in my life.

Table of Contents

List of Symbols ……v

Chapter 1: Introduction ……1
1.1 Description of Vortex Induced Vibration ……1
1.2 Motivation of the Research ……5
1.3 Overview of the Thesis ……6
1.4 Background ……7
1.5 CFD Model ……10

Chapter 2: Comparison of Results ……15
2.1 Procedure ……15
2.2 Krenk and Nielson Model ……17
2.3 Facchinetti, de Langre, and Biolley Model ……25
2.4 Lin Model ……41
2.5 Farshidianfar and Zanganeh Model ……47

Chapter 3: Analysis of Results ……53
3.1 General Discussion ……53
3.2 Analysis of Nonlinearity of the Wake Equation ……56

Chapter 4: Conclusion ……60
4.1 Review of Results ……60
4.2 Future Work ……61

Bibliography ……63

List of Symbols

A,B	Tunable Parameters
C_D	Drag Coefficient
C_L	Lift Coefficient
$C_{L,0}$	Lift Coefficient for Fixed Cylinder
C_M	Added Mass Coefficient
c_0	Coupling Coefficient
D	Cylinder Diameter
f	Strouhal Frequency in Hertz
L	Cylinder Length
M	Mass Number
m_0	Cylinder Mass and Added Fluid Mass
m_f	Fluid Mass
$m_{f,0}$	Added Fluid Mass
q	Non-dimensional Wake Variable
q_0	Non-dimensional Wake Variable for Fixed Cylinder
Re	Reynolds Number
S_G	Skop-Griffin Parameter
St	Strouhal Number
T	Dimensional Time

t	Non-dimensional Time
U	Uniform Flow Velocity
U_r	Non-dimensional Reduced Flow Velocity
w	Transverse Motion of a Representative Fluid Mass
w_0	Transverse Motion of Fluid Mass for Fixed Cylinder
x	Dimensional Cylinder Displacement
y	Non-dimensional Cylinder Displacement
α	Stall Parameter
γ	Non-dimensional Coupling Parameter
δ	Frequency Ratio of Structural Frequency to Fluid Frequency
ε	Tunable Parameter
ζ	Viscous Damping Ratio
ζ_f	Fluid Damping Ratio
ρ	Fluid Density
μ	Mass Ratio of Structural Mass to Fluid Mass
μ_f	Mass Ratio of Fluid Mass to Structural
ω_0	Structural Natural Frequency
ω_s	Vortex Shedding Frequency
υ	Kinematic Viscosity

Chapter 1

Introduction

1.1 Description of Vortex Induced Vibration

Vortex-induced vibration (VIV) is a phenomenon that can exist when there is fluid flow over a bluff body. Many different kinds of long slender structures experience VIV including chimneys, suspended bridge cables, power transmission lines, underwater pipes, and legs and cables of offshore structures [6]. As the fluid flows over a bluff body, a boundary layer forms, and as the Reynolds number (*Re*) increases, the boundary layer separates and vortices are formed. These vortices shed alternately from the upper and lower part (or left and right in the case of a vertical member) of the rear of the body and are called the Kármán vortex streets. They are named after von Kármán who explained this stable alternating vortex pair configuration in a paper published in 1911 [8]. The vortex street occurs in most bluff-body flow situations for $Re > 35$ and persists over a wide range of Reynolds numbers [21]. The alternating vortex pair configuration creates an alternating lift force which acts in the transverse direction to the fluid flow. If the structure is flexible, this lift force induces structural motion that is also transverse to the direction of the fluid flow, which can result in fatigue over time, a primary cause of damage. There is also a drag force on the bluff body that causes motion parallel to the flow, but this will not be considered in the simple models addressed in this thesis.

When describing VIV it is possible to solve the Navier-Stokes equation subject to the appropriate boundary and initial conditions using computational techniques. This is desirable if

the computational tools are available and knowledge of the entire flow field as well as the motion of the structure is desired; however, if only the behavior of the bluff body is of interest it may be sufficient to model the fluid-structure interaction using a simpler, reduced order phenomenological model to limit computational time and complexity. These simpler models may also shed some light on the underlying physics of the system. A common way to model a simple bluff body in fluid flow is as a two degree of freedom (dof) system, where one dof describes the motion of the structure and the other the fluctuating lift force or coefficient [12]. In the literature, the bluff body is generally assumed to be a one degree of freedom, elastically supported, rigid right circular cylinder that is constrained to oscillate transverse to the uniform flow. A physical model of the system described above is shown in Figure 1.1.

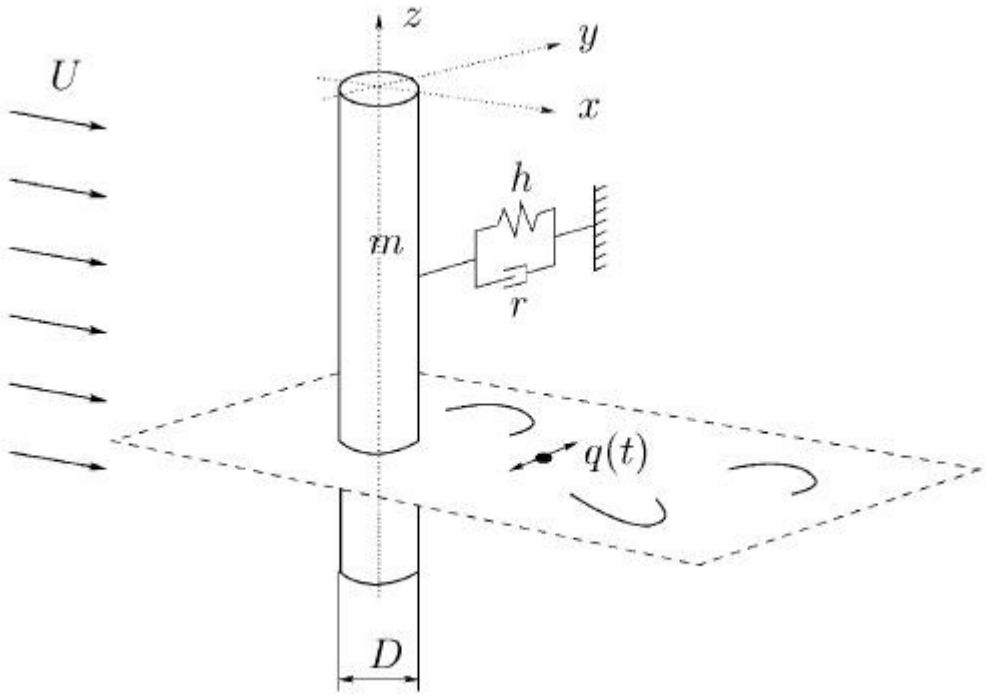

Figure 1.1: Physical model of right circular cylinder in fluid flow [6].

In this model, *h* is the cylinder stiffness coefficient, *r* is the cylinder damping, and *m* is the cylinder mass. The other variables include *U*, the uniform flow velocity, *D*, the cylinder diameter, and *q(t)*, a flow variable that can be related to the fluctuating lift coefficient.

Given the physical model in Figure 1.1, the structural oscillator is modeled as a linear oscillator with mass, damping, and stiffness directly coupled to the fluid oscillator. The fluid oscillator that describes *q(t)* is assumed to be a non-linear system that exhibits limit cycle behavior, such as a van der Pol or Rayleigh oscillator, seen in equations 1.1 and 1.2 respectively. The fluid oscillator may also exhibit instability through a negative damping term. A number of different models, a variety of coupling methods between the fluid and structure, as well as several non-linear structural oscillators, will be examined in a later chapter.

$$\ddot{q} - \varepsilon(1 - q^2)\dot{q} + q = 0 \tag{1.1}$$

$$\ddot{q} - \varepsilon(1 - \dot{q}^2)\dot{q} + q = 0 \tag{1.2}$$

It is important when studying VIV to consider the Strouhal relationship between the vortex shedding frequency, flow velocity, cylinder diameter, and non-dimensional Strouhal number *St*. The Strouhal relationship is given by

$$St = fD/U \tag{1.3}$$

The Strouhal number varies with Reynolds number, but is approximately equal to 0.2 for Reynolds numbers from 300 to 10^5 [21]. It will be shown later that a Reynolds number of 100 is desirable for the models considered in this thesis, so a Strouhal number less than 0.2 will be employed here.

An important phenomenon that is seen in VIV is lock-in or synchronization. Outside of lock-in the frequency of vibration of the cylinder matches the vortex shedding frequency, which

is defined by the Strouhal relationship given in equation 1.3. When the vortex shedding frequency approaches the natural frequency of the structure, the system enters lock-in and the vortex shedding frequency no longer follows the Strouhal relationship but instead jumps to the natural frequency of the structure [1]. This causes the frequency of vibration to match the natural frequency of the structure. During lock-in the structural oscillations drastically increase in amplitude. This is the region where fatigue is most likely, as the system undergoes large amplitude vibrations. A plot showing how frequency of oscillation varies with flow velocity is given in Figure 1.2.

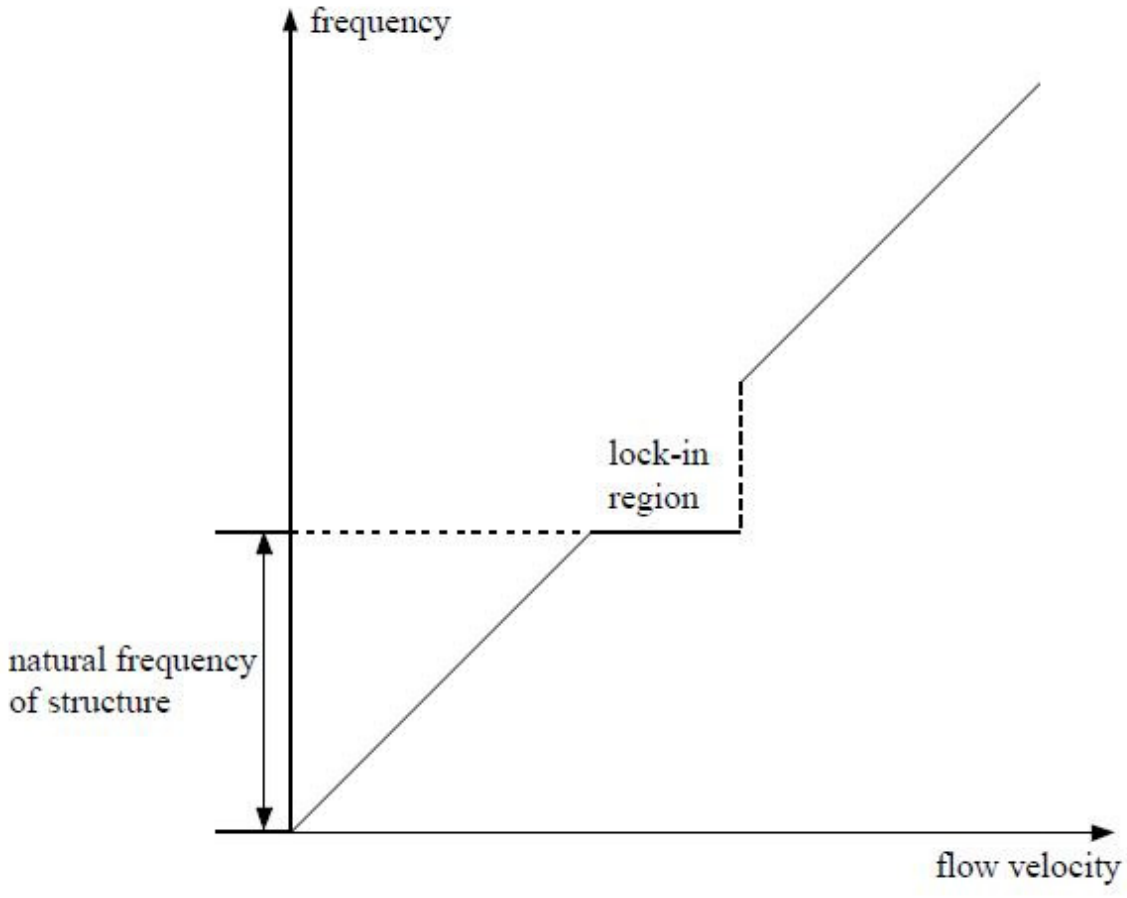

Figure 1.2: Plot of vortex shedding frequency vs. flow velocity [1].

As Figure 1.2 shows, the shedding frequency increases with flow velocity up to the point where the system enters lock-in. Once in the lock-in region, the shedding frequency no longer changes with flow velocity but instead matches the natural frequency of the structure. As the flow velocity continues to increase, the system exits the lock-in region, and the shedding frequency again increases with flow velocity.

1.2 Motivation of the Research

Research in vortex-induced vibration has been ongoing for many years, and finding a reduced order model to describe the behavior of even this simple system has been a challenge. There are two different methods that are often used to develop reduced order models; one uses simulation or experimental data to construct the model (i.e., a data-driven model), and the other employs an ad hoc phenomenological model that broadly replicates features of VIV with sufficient free parameters that can be "tuned" to provide some degree of agreement with data. Constructing data-driven reduced order models is an ongoing goal of our research group but is quite challenging. Further discussion of this approach to the VIV problem will be left to others. In this thesis, only existing phenomenological models, documented since the early work of Birkoff and Zarantanello (1957) and Bishop and Hassan (1964), will be addressed [2], [3]. Many such models have been developed in an attempt to accurately predict the structural response of a system undergoing VIV. These different models encompass a variety of constructions, which cause them to exhibit different behaviors. By comparing the performance of each of them to the limited experimental data available, it is difficult to determine which model provides the best predictions over broad ranges of parameters. In this thesis, several of these

models will be compared with results from a high fidelity finite element Navier-Stokes solver, incorporating the sprung bluff-body, allowing careful comparison of solution features not possible with experimental data alone. Once the efficacy of each reduced order model is evaluated, the best of them can be utilized to better understand the physics of VIV.

1.3 Overview of the Thesis

This research focuses on a number of different phenomenological models that have been developed over the years to study vortex-induced vibration. Starting with the early work by Birkoff and Zarantanello (1957) and Bishop and Hassan (1964) and continuing through the most recent contributions, the literature of reduced order models will be examined and explained. Several models will then be examined more closely and directly compared with high-fidelity CFD results obtained within our group. These models include a number of different equation types and couplings, for which a detailed explanation is given in Chapter 2.

Also in Chapter 2, each of these models is compared with the results of numerical simulation. The procedure for this is explained in 2.1. In each model, physical parameters such as mass ratio and frequency are fixed, and the remaining parameters are considered tunable. The structural motion and lift coefficient predicted by each will be compared with the simulation results. The frequency response of the cylinder, corresponding to each model is examined to see if it matches observed results for the computational system. The cylinder amplitude versus Reynolds number is determined for each model and compared with the simulation result. This comparison will demonstrate how the system responds around the lock-in region. Finally, the structural damping of each model will be determined and compared with

the simulation data by using a Griffin plot. Once all of these models are examined and compared with the simulation results, we will be able to conclude to what extent the reduced order models correctly predict the features of VIV.

Chapters 3 and will review the efficacy of the various reduced order models in describing VIV, and an overview of the results will be presented, along with conclusions and recommendations regarding the quality of the individual model predictions. Finally, in Chapter 4, recommendations for future studies will be presented.

1.4 Background

Vortex induced vibration (VIV) of sprung right-circular cylinders in cross flow has been studied for many years with the motivation of finding a reduced-order model that accurately predicts both cylinder and fluid behavior. Studies of phenomenological models have been conducted following the early work of Birkoff and Zarantanello (1957) and Bishop and Hassan (1964). Bishop and Hassan are often credited with first suggesting a fluid oscillator with non-linear self-excited behavior [8], basically a van der Pol oscillator. Bishop and Hassan drew many conclusions about the physics of VIV that will be shown to be true later in this thesis. They introduced the idea of lock-in or, as they called it, the "range of synchronization." They also observed the change in amplitude and phase upon entering lock-in, noting that this occurred as a sudden jump at a certain critical frequency. Hysteresis was also observed, meaning that the critical frequency of lock-in depends on whether the frequency is increasing or decreasing [3].

Hartlen and Currie (1970) presented one of the earliest wake oscillator models. It is a basis for much of the later work done on VIV. Their model consisted of a linear structural

oscillator coupled to a nonlinear wake oscillator. The wake oscillator was modeled as a nonlinear-oscillator. The non-dimensional equations of motion of this model are

$$y'' + 2\zeta y' + x = A\omega_0^2 C_L \tag{1.4}$$

$$C_L'' - \frac{\varepsilon}{\delta} C_L' + \gamma\delta(C_L')^3 + \left(\frac{1}{\delta}\right)^2 C_L = Bx' \tag{1.5}$$

As equation 1.5 shows, a Rayleigh oscillator is used to model the fluid, which has the self-excited behavior sought. The wake oscillator is coupled to the structural oscillator by a velocity term, and the lift coefficient couples the structure to the fluid. This type of coupling will be considered more closely when looking at one of the Facchinetti model variants. This system resembles many of the models that will be discussed in more detail in the next section and exhibits some fundamental behavior of VIV. Frequency lock-in is seen in this model along with large cylinder amplitude oscillation during lock-in. Hysteresis is also observed in this model, and different critical frequencies are observed depending on the direction of the frequency sweep.

The contributions of Skop and Griffin (1973) are also very significant in the study of VIV. They also used a limit cycle oscillator to model the fluid and a linear structural oscillator for the cylinder. The primary difference between this model and the one proposed by Hartlen and Currie is the method by which some of the model parameters are derived. They related their model parameters to the physical parameters of the system as opposed to leaving them free to tune to data. Skop and Griffin do capture some of the effects of VIV, including a phase shift during lock-in and the amount of energy transferred during maximum cylinder vibration amplitude. Another major contribution by Skop and Griffin is their combined mass-damping parameter called the Skop-Griffin parameter,

$$S_G = 8\pi^2 St^2 \mu\zeta \tag{1.6}$$

an important parameter when considering damping in the system. A Griffin plot (Khalak and Williamson, 1999) graphs the structural amplitude at lock-in versus the Skop-Griffin parameter, a valuable tool in studying VIV [11]. This will be discussed in more detail later on.

Another model, by Iwan and Blevins (1974) develops the fluid oscillator equation from the fluid mechanics of the vortex street. This model is given in terms of a fluid variable other than the lift coefficient. The notion of a fluid variable is used in many of the models that are more closely examined in this thesis. The forms of the equations are similar to those of the other models that have been considered, however, the parameters are derived from experimental data for fixed and harmonically forced cylinders. Once the parameters are found, the equations are used to predict the motion of a rigid elastically mounted cylinder.

A more recent model by Skop and Balasubramanian (1997) introduces a stall term to provide asymptotic, self-limiting structural response at zero structural damping. The stall term is related to the velocity of the cylinder and is given by

$$C_L(x,t) = q(x,t) - \frac{2\alpha}{\omega_s}\dot{y}(x,t) \tag{1.7}$$

In this equation, $q(x,t)$ is taken to satisfy the van der Pol equation, and α is to be determined from experimental results. The second term on the right hand side of equation 1.7 implies that the magnitude of the lift force decreases for large structural oscillations, so this is the stall term. The final equations of motion are

$$\ddot{y} + 2\zeta\omega_0\dot{y} + \omega_0^2 y = \mu\omega_s^2\left(q - \frac{2\alpha}{\omega_s}\dot{y}\right) \tag{1.8}$$

$$\ddot{q} - \omega_s G(C_{L0}^2 - 4q^2)\dot{q} + \omega_s^2 q = \omega_s F\dot{y} \tag{1.9}$$

The lift force is seen on the right hand side of equation 1.8; this is where the stall term enters. If the cylinder velocity term, or stall term, from the right hand side is moved to the left hand side,

then even if the structural damping is zero the cylinder will have some damping to limit the response. The introduction of a stall term has been employed since its use by Skop and Balasubramanian, and it's an important feature of models that will be closely analyzed here such as those by Facchinetti.

Another approach that should be considered in future studies, but is not considered here, is one by Ogink and Metrikine (2008, 2010) [16], [17]. In this model the coupling between the structure and fluid oscillators is written as a convolution integral. This allows the coupling to be frequency dependent. The parameters are tuned based on forced vibration measurements, where the cylinder is forced to vibrate at a certain amplitude and frequency. These parameters are fixed, and the model is used to simulate free vibration. At this point, the results from this approach have not yielded acceptable results, but this method should be researched further as it is relatively new.

1.5 CFD Model

A computational fluid dynamics (CFD) model that is used to describe vortex-induced vibration is of great importance in this study. The results of this model are used as the benchmark for comparing the reduced order models and testing the quality of each one. The domain of the finite element model is seen in Figure 1.3, and its dimensions are $48D \times 24D$, where D is the cylinder diameter. The fluid enters the domain only moving in the x-direction and the cylinder is constrained to move only in the y-direction. The mesh for this model is seen in Figure 1.4.

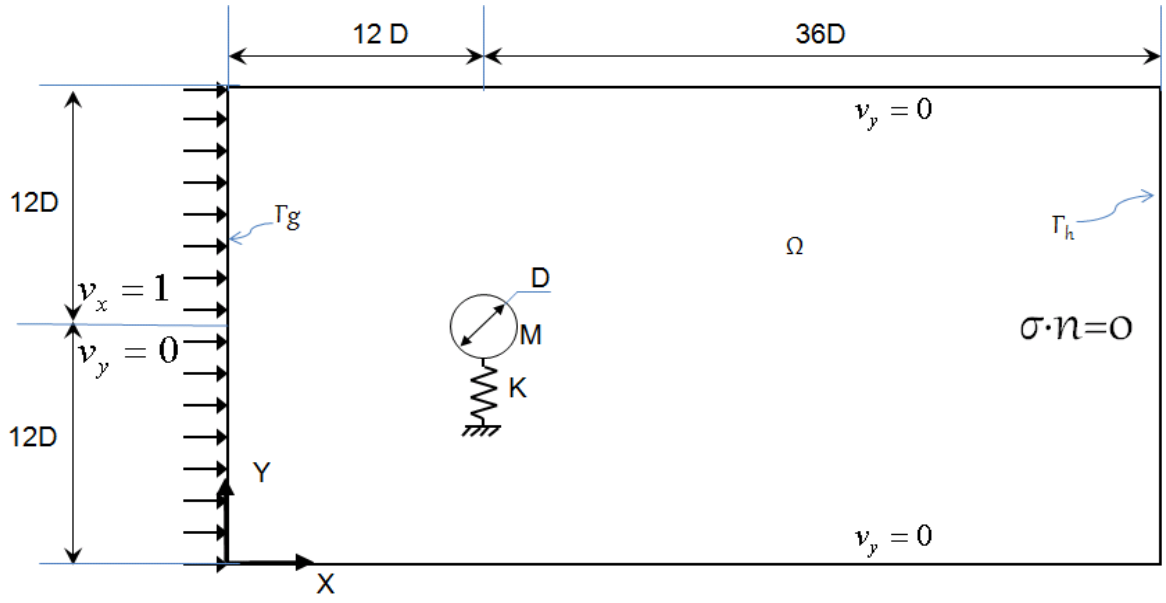

Figure 1.3: Domain of the finite element model.

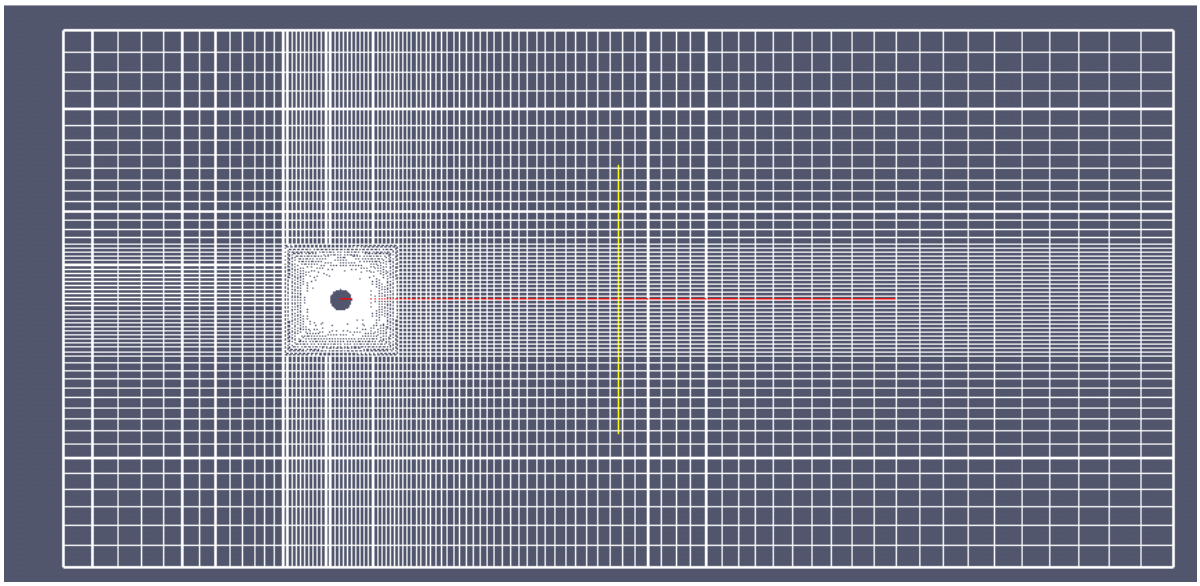

Figure 1.4: Mesh of finite element domain.

The mesh has a higher density near the cylinder, so the elements close to the cylinder are smaller than the elements far from it. The total number of nodes in this model is 8461 and the total number of elements is 8261 [4], [15].

The structural response of the CFD model at lock-in, normalized by the cylinder diameter, is seen in Figure 1.5. The steady state amplitude of the plot is 0.5 and the frequency is equal to the natural frequency of the cylinder, which is 1.05. The reduced order models will be tuned to try to match this plot.

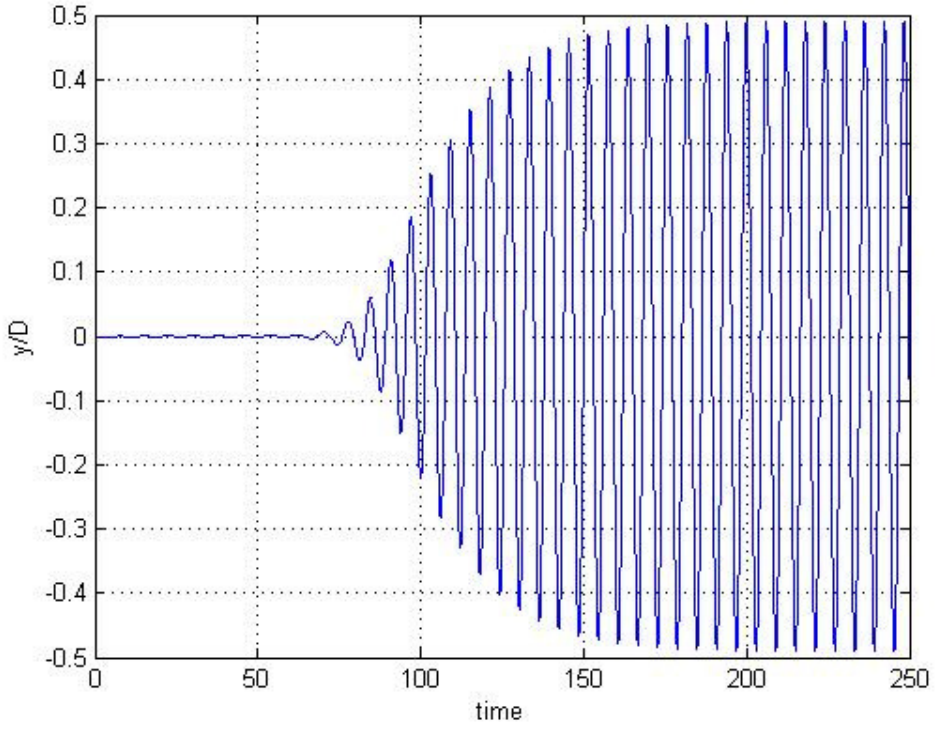

Figure 1.5: Non-dimensional cylinder displacement vs. time for CFD model.

The lift coefficient time series will be difficult to emulate; it can be seen in Figure 1.6. It increases to 0.4 initially, but over time it settles to 0.2, which is difficult behavior for a reduced order model to capture. It will be shown later that many of the models will overestimate the lift coefficient during lock-in, though the lift coefficient vs. *Re* plot, seen in Figure 1.7, might be able to explain this.

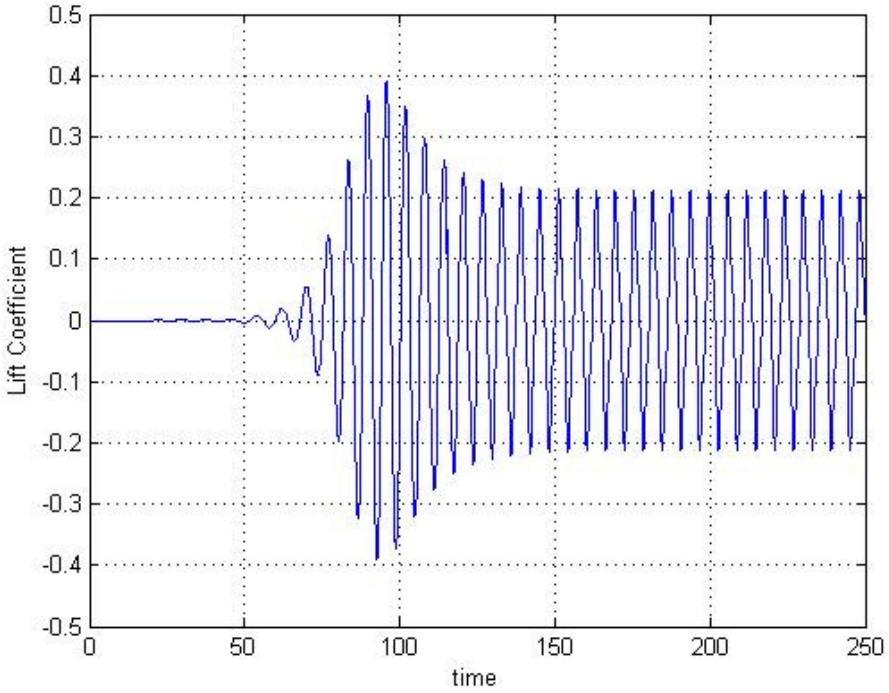

Figure 1.6: Lift coefficient vs. time for CFD model.

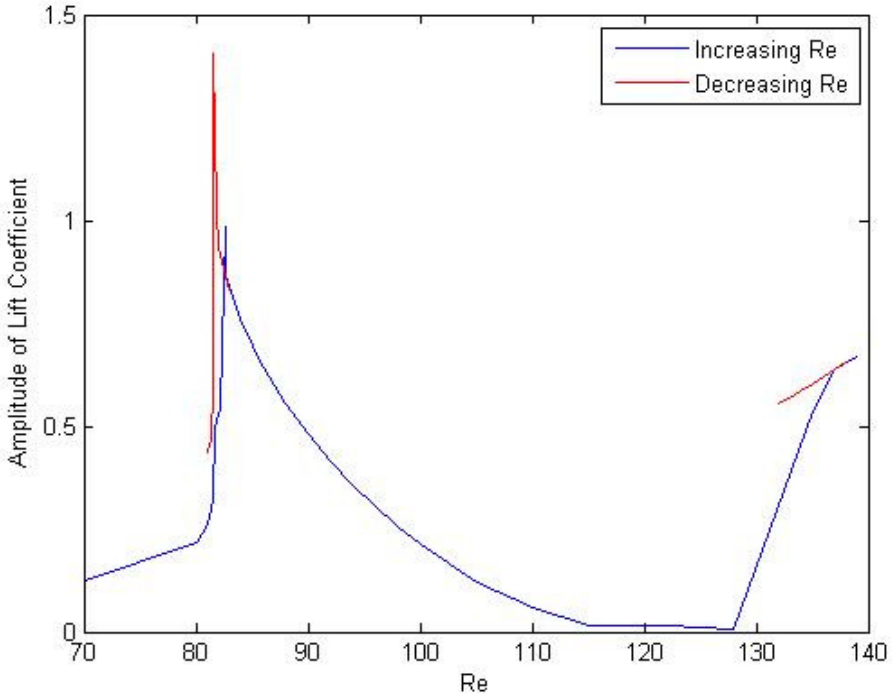

Figure 1.7: Lift coefficient vs. *Re* for CFD model.

As Figure 1.7 shows, when the system first enters lock-in, the lift coefficient jumps to a value above 1, but throughout lock-in the lift coefficient decreases and approaches 0. This decreasing behavior will be shown to be difficult to model successfully with a reduced order model. The structural amplitude vs. *Re* is another important plot, shown in Figure 1.8.

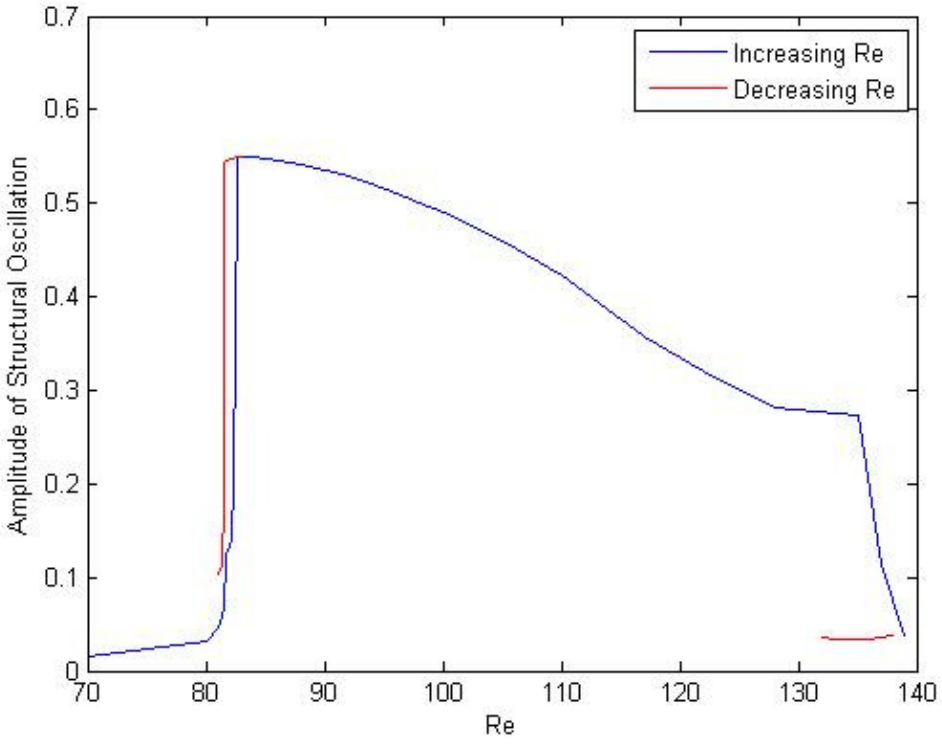

Figure 1.8: The steady-state structural amplitude vs. Reynolds number for the CFD model.

This plot shows amplitude amplification throughout lock-in and hysteresis at the beginning and end of lock-in. An attempt will be made to reproduce all of these results when studying the reduced order models, and a comparison between these models and the CFD results will ultimately determine the quality of each reduced order model.

Chapter 2

Comparison of Results

2.1 Procedure

Several models will now be discussed in detail, closely analyzed, and compared with the high fidelity finite element model developed in our group for vortex-induced vibration studies. Each of these systems of equations will be solved in Matlab™ using the ode45 solver, a Runge-Kutta method. For each model there are parameters within the equations that can be tuned in order to match experimental response data. In this study, these parameters are tuned to match numerical simulation results. More to the point, the parameters are tuned to best match the steady-state structural amplitude, frequency, and lock-in region of the CFD results. The tuning process and parameter values will be discussed in more detail for each individual model.

Once the parameters are appropriately tuned, a comparison of results from the different reduced order models and the CFD model is conducted. One result that we compare is the time series for the motion of the structure. The amplitude and frequency of the time series at lock-in will be compared with those of the time series obtained from numerical simulation. The results will be presented as non-dimensional amplitude, *y/D*, vs. *time* and non-dimensional amplitude vs. Reynolds number over the lock-in range. The equation for the Reynolds number is

$$Re = \frac{UD}{\upsilon}. \tag{2.1}$$

For the CFD model, the nominal value of *Re* is taken to be 100, so the same will be applied to the reduced order models. Assuming nominal values of *U*=1 and *D*=1, the kinematic viscosity

must be υ=0.01 for *Re*=100 to be achieved. This plot will show the structural amplitude at lock-in, the range of lock-in, and whether or not hysteresis is seen at the beginning and end of lock-in. The time-varying lift coefficient will also be compared. Note that the parameters are tuned to match the structural time series most closely; thus, the lift coefficient is free to do what the data dictates. Because of this, the lift coefficient results may not match well.

Another valuable result is the Griffin plot; it shows the log-log relationship between the maximum structural amplitude and the Skop-Griffin parameter, which is a combined mass-damping parameter, and is defined by equation 1.6. At *Re*=100, *St*=0.167 [21]. The results should show that, as the damping ratio or mass ratio increase, the maximum structural amplitude decreases. Comparing each reduced order model is also beneficial, and the type of coupling between the fluid and the structural oscillators should be studied. Some of the models use three different types of coupling, displacement, velocity, and acceleration, and finding the best of these is one of the goals of this research. The form of the structural oscillator also varies between the models; two of the models, Facchinetti el al. (2004) and Krenk and Nielsen (1999), use a linear oscillator to represent the structure while the other two, Farshidianfar and Zanganeh (2010) and Lin et al. (2009), contain some nonlinearity in the structural oscillator. Finally, the type of nonlinearity in the wake oscillator can be compared. The van der Pol oscillator is often used here, but in Krenk and Nielsen (1999) a combination of a van der Pol and Rayleigh oscillators is used. It has been hypothesized that the exact type of nonlinearity does not matter, as long as it exhibits the desired limit cycle behavior.

2.2 Krenk and Nielsen Model

The first model considered is that of Krenk and Nielsen (1999). In this model, the two oscillators represent the motion of the structure and the fluid mass. The fluid variable is a generalized displacement which can be related to the lift coefficient, as shown later on. The coupling in this model is based on energy flow between the fluid and the structure, so the forcing terms correspond to flow of energy. These ideas lead to response characteristics matching that of those observed in vortex-induced vibration experiments as well as in the CFD model. These characteristics include lock-in around the structural natural frequency, amplitude amplification at lock-in, and the two branches being separated by a 180° phase difference. Even though some of the characteristics between this model and the CFD model match, others do not; this correspondence will all be discussed.

The following equations of motion are used to describe the mechanics of this model. The structural oscillator is assumed to be a classical damped linear oscillator forced by a time dependent lift coefficient and is given by

$$m_0(\ddot{x} + 2\zeta\omega_0\dot{x} + \omega_0^2) = \frac{1}{2}\rho U^2 C_L DL. \tag{2.2}$$

The lift coefficient is related to the transverse velocity of the fluid mass by

$$C_L(t) = \frac{\dot{w}}{U}\gamma \tag{2.3}$$

where γ is taken to be a constant in this model. The dimensional structural oscillator can then be written as

$$m_0(\ddot{x} + 2\zeta\omega_0\dot{x} + \omega_0^2 x) = \frac{1}{2}\rho UDl\dot{w}(t)\gamma \tag{2.4}$$

In the fluid oscillator, the nonlinear term is a combination of van der Pol and Rayleigh oscillators, showing that a more general nonlinear fluid damping term can be applied. The frequency of this oscillator is taken to be the shedding frequency, ω_s, of the vortices from the bluff body which can be found from the Strouhal relation,

$$\omega_s = 2\pi(St)U/D. \tag{2.5}$$

In this relation *St* is about 0.2 for a wide range of Reynolds numbers, but in this case *Re*=100 giving *St*=0.167. The forcing of the fluid oscillator is provided by the velocity of the cylinder, so the rate of energy transfer from the fluid to the cylinder is identical to that of the cylinder to the fluid. The equation for the dimensional fluid oscillator is

$$m_f\left[\ddot{w} - 2\zeta_f\omega_s\left(1 - \frac{w^2+\dot{w}^2/\omega_s^2}{w_0^2}\right)\dot{w} + \omega_s^2 w\right] = -\frac{1}{2}\rho U D l\dot{x}(t)\gamma \tag{2.6}$$

where m_f is proportional to the fluid mass density and the volume of the structure. The parameter w_0 controls the amplitude of the vibrations of the fluid, and ζ_f is related to the sensitivity of the energy source to changes in the fluid oscillation amplitude.

The energy flow over a period for this system starts with energy generation by the negative damping term in the fluid oscillator which is then extracted by the right hand side of equation 2.6. The energy is then transferred to the cylinder by means of the right hand side of equation 2.4, and if the cylinder has some damping the energy is finally dissipated in the cylinder. This energy flow condition is what makes this model unique when compared with other double oscillator models that are examined in this thesis.

Finally, these equations can be non-dimensionalized. The structure and fluid oscillators can be described by two non-dimensional variables, y and q, given by

$$y = \frac{x}{D} \tag{2.7a}$$

$$q = \frac{w}{w_0} \tag{2.7b}$$

The fluid amplitude parameter w_0 can be represented in non-dimensional form as

$$q_0 = \frac{w_0}{D} \tag{2.8}$$

The mass ratio of the system can be described as the mass of the fluid divided by the mass of the cylinder.

$$\mu_f = \frac{m_f}{m_0} = \frac{\rho D^2 l}{m_0} \tag{2.9}$$

After making these substitutions, the coupled non-dimensional differential equations can be written as

$$\ddot{y} + 2\zeta_0\omega_0\dot{y} + \omega_0^2 y = \mu_f c_0 \omega_s \dot{v} \tag{2.10}$$

$$\ddot{q} - 2\zeta_f\omega_s[1 - q^2 - (\dot{q}/\omega_s)^2]\dot{q} + \omega_s^2 q = -q_0^{-2} c_0 \omega_s \dot{y} \tag{2.11}$$

where the coupling coefficient is given by

$$c_0 = \frac{C_{L,0}}{2(2\pi St)^2}. \tag{2.12}$$

The first step in comparing this model with simulation data is to define the tunable parameters and find their values so the structural oscillator best fits the CFD results. Referring to equations 2.10 and 2.11, the different parameters can be assigned values based on those used in the CFD model and then tuning to match results. In these equations, $\zeta = 0$, $\omega_0 = 1.05$, and $\mu_f = 0.1$ since these were the values used in the CFD model. The fluid frequency is $\omega_s = 1.05$, since frequency lock-in is the area of interest. The remaining parameters are considered to be tunable; those are c_0, v_0, and ζ_f where, from Krenk and Nielsen (1999), $c_0 = v_0$. This results in two parameters that are adjusted, iteratively, until structural oscillation

results match the CFD results for the motion of the cylinder as closely as possible. The final values are $c_0 = v_0 = 1.75$ and $\zeta_f = 0.01$.

Incorporating these parameter values, Figure 2.1 shows the structural displacement for the Krenk and Nielsen model and the CFD model.

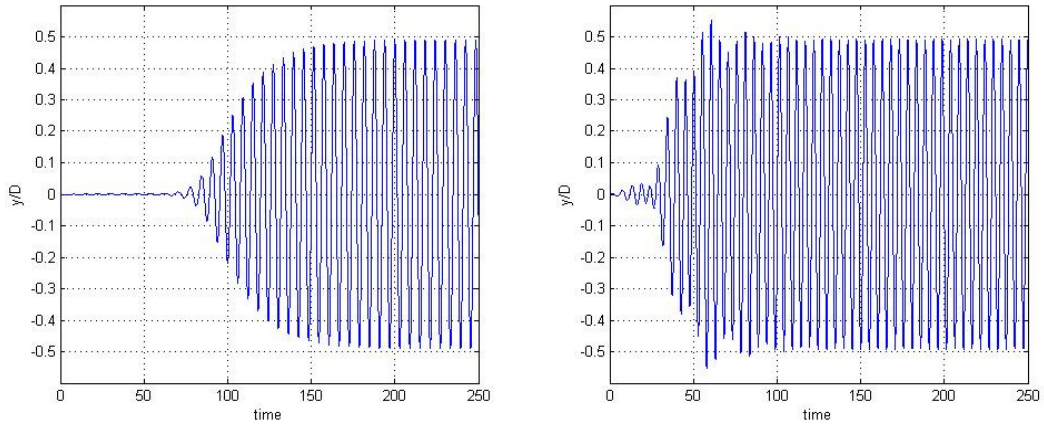

(a) CFD model results (b) Krenk and Nielsen Model

Figure 2.1: Non-dimensional cylinder displacement vs. time for CFD model and Krenk and Nielsen model.

As these plots show, after tuning the parameters the steady state structural amplitude of these two models matches. A major difference in these plots is the transition from low amplitude to the steady state. Figure 2.1a shows a slow increase to the steady state amplitude with no overshoot, while Figure 2.1b shows a faster jump in amplitude and some initial overshoot. This difference may be an indication of other major problems this model may encounter. Since some of the parameters of the model were adjusted to match the steady state structural amplitude, this positive result is not surprising. More interesting results will be seen while observing the lift coefficient and the frequency behavior of this model, since these were not directly controlled by tuning the parameters.

The lift coefficient is essentially the driving force on the cylinder and Figure 2.2 shows it for this model compared with the CFD model.

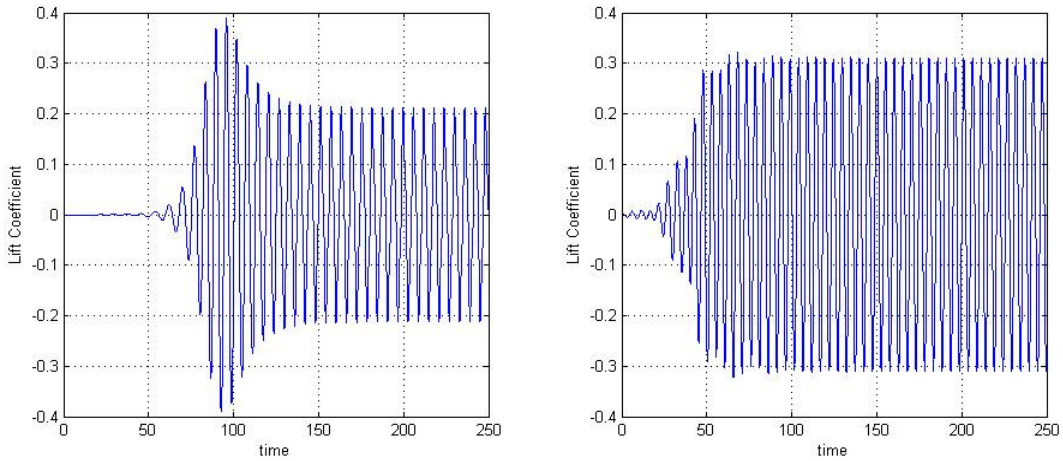

(a) CFD Model (b) Krenk and Nielsen Model

Figure 2.2: The lift coefficient vs. time for the CFD model and the Krenk and Nielsen Model.

As Figure 2.2 shows, the steady state lift coefficients do not precisely match. The CFD results are very interesting as the lift coefficient increases to 0.4 but then decreases and settles at 0.2. The Krenk and Nielsen model has simpler behavior as the lift coefficient increases to approximately 0.3 and remains there. The lift coefficient not matching is a feature of many of the models studied here; this will be explored further when studying the Facchinetti model.

The frequency behavior of each model is also very important. It is well known that when the vortex shedding frequency is far from the natural structural frequency of the cylinder the cylinder vibrates at the Strouhal frequency; however, as the vortex shedding frequency approaches the natural structural frequency, it locks in and the vortex shedding and cylinder vibration frequencies match that of the natural structural frequency. Figure 2.3 shows the frequency behavior of the Krenk and Nielsen model.

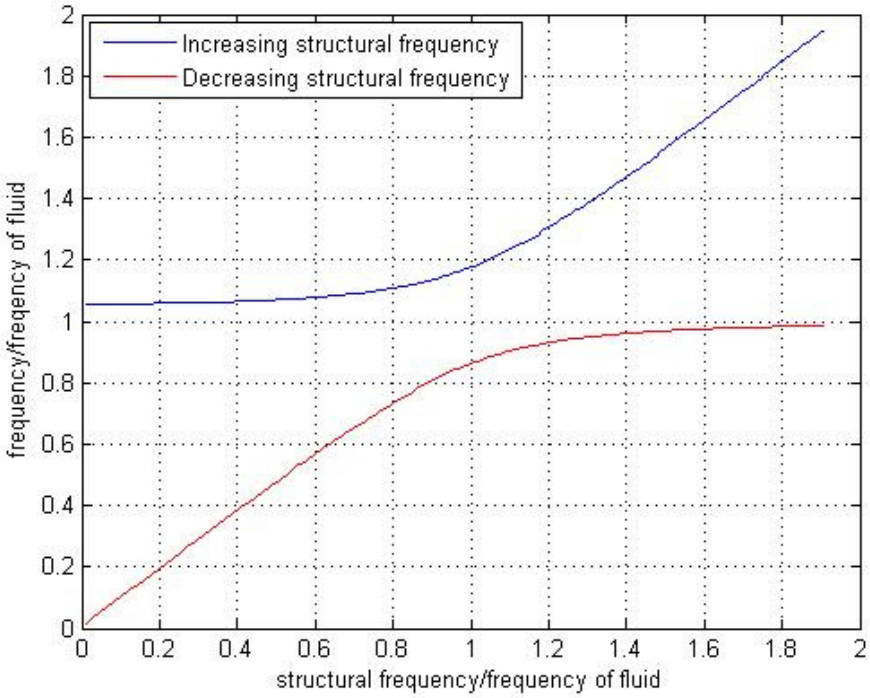

Figure 2.3: The frequency of vibration of the cylinder vs. the natural structural frequency normalized by the frequency of the vortex shedding for Krenk and Nielsen.

Figure 2.3 is plotted to show the effect of changing the structural frequency, but this is the same as changing the fluid frequency in the opposite direction. In this plot both the frequency of vibration and the structural frequency are normalized by the frequency of the fluid, which is also known as the Strouhal frequency and defined by equation 2.6. There are two modes seen in this system, one corresponding to increasing structural frequency and the other corresponding to decreasing structural frequency. For each branch the system starts out not in lock-in so it approximately tracks the Strouhal frequency; however, once it approaches the structural frequency, it locks onto a frequency nearby. There are a couple problems with this model's frequency response; one is that once a branch locks on to the structural frequency it seems to never leave exit lock-in which is not consistent with known results, where the system

eventually does return to the Strouhal frequency. Another problem is that it never locks on to the exact structural frequency of the system but instead it seems to jump to a nearby frequency and slowly converge to the structural frequency. This problem indicates a fundamental difference between the Krenk and Nielsen model and the CFD model since, in the latter, at lock-in the response frequency matches the natural frequency of the cylinder.

Another important plot to look at is the structural amplitude vs. Reynolds number to see how the amplitude evolves with increasing and decreasing Reynolds number. Figure 2.4 shows the CFD and Krenk and Nielsen results.

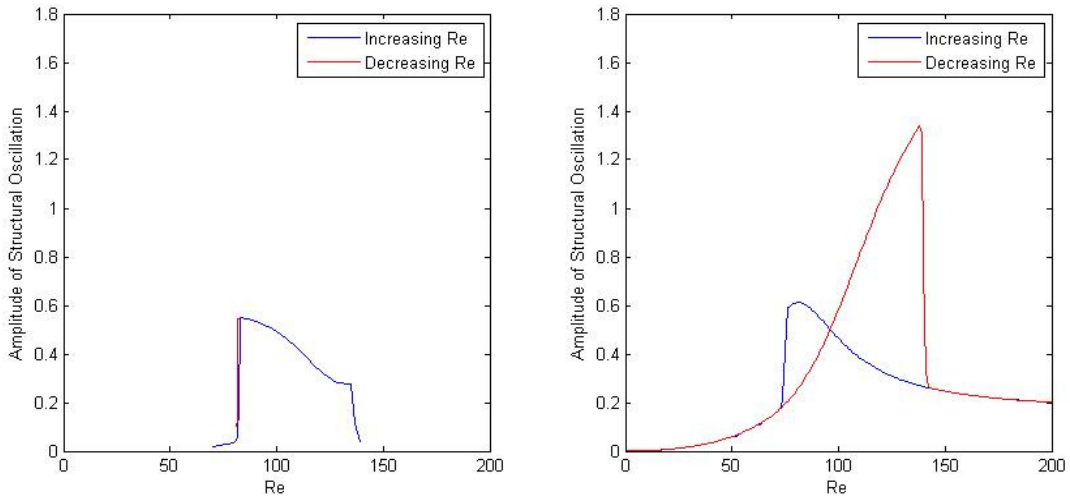

(a) CFD Model (b) Krenk and Nielsen Model

Figure 2.4: The steady state structural amplitude vs. Reynolds number for increasing and decreasing Reynolds number.

As Figure 2.4 shows, these results differ significantly, and this indicates that the Krenk and Nielsen model is not best suited to match the CFD results at Reynolds numbers around 100. *Re*=100 corresponds to identical structural and fluid frequencies, and this is where the parameters are tuned to match the amplitudes of the structural time series; thus, these plots match at this point, but not at most other points. Both of these plots show a region of lock-in

where the amplitude is magnified, but the Krenk and Nielsen model shows two distinct branches of the solution while the CFD model shows overlapping solutions with hysteresis at the beginning and end of lock-in. The Krenk and Nielsen model also over-predicts the displacement magnification during the lock-in regime, predicting a value as high as 1.4.

The Griffin plot, which gives the structural amplitude vs. the Skop-Griffin parameter, is a useful plot to consider while studying vortex-induced vibration. The Skop-Griffin parameter is defined by equation 1.6, and the Griffin plot for the Krenk and Nielsen model and the CFD model can be seen in Figure 2.5.

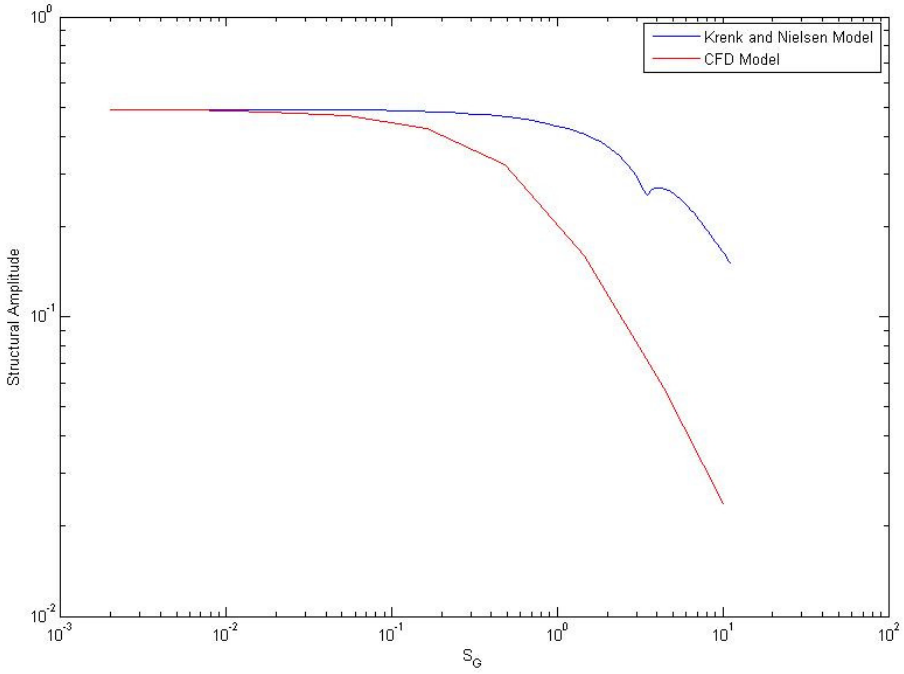

Figure 2.5: Griffin plot for the Krenk and Nielsen model and CFD model.

The Skop-Griffin parameter increases with structural damping so it makes sense that as this parameter increases, the structural amplitude decreases. Figure 2.5 shows a significant

difference between the two models as the CFD model's structural amplitude decreases much faster than that of the Krenk and Nielsen model.

2.3 Facchinetti, de Langre, and Biolley Model

The next model considered in this study is that of Facchinetti, de Langre, and Biolley (2004). This model, like all the models considered herein, consists of a structural oscillator and a fluid oscillator. The structural oscillator is again the damped linear oscillator, while the fluid oscillator is chosen to be a van der Pol oscillator, because of its limit cycle behavior. Three types of coupling are considered in this model; displacement, velocity, and acceleration. All three are examined, but it is shown that acceleration coupling leads to best fits in the VIV data, qualitatively and quantitatively.

The structural oscillator has a mass component from the cylinder and from the fluid, along with a damping component of the cylinder and of the fluid. The equations for the total mass and mass ratio are

$$m = m_s + m_f \qquad m_f = C_M \rho D^2 \pi / 4 \qquad \mu = (m_s + m_f)/\rho D^2 \qquad (2.13a,b,c)$$

The structural oscillator takes the form

$$\ddot{x} + \left(2\zeta\omega_0 + \frac{\gamma}{\mu}\omega_s\right)\dot{x} + \omega_0^2 x = S/m \qquad (2.14)$$

where S is a forcing term that will be discussed later.

The wake model is the van der Pol oscillator with the three aforementioned forcing terms considered

$$\ddot{q} + \varepsilon\omega_s(q^2 - 1)\dot{q} + \omega_s^2 q = F. \qquad (2.15)$$

Here, then, F is the forcing function controlled by the displacement, velocity, or acceleration of the structure. The wake variable q can be related to the fluctuating lift coefficient by the expression

$$C_L = \frac{1}{2} C_{L,0} q \tag{2.16}$$

where $C_{L,0} = 0.3$.

Equations 2.14 and 2.15 are converted to dimensionless form using the non-dimensional variables

$$y = x/D \tag{2.17a}$$

$$t = T\omega_s \tag{2.17b}$$

When these expressions are substituted into the equations of motion, the non-dimensional model takes the form

$$\ddot{y} + \left(2\zeta\delta + \frac{\gamma}{\mu}\right)\dot{y} + \delta^2 y = s' \tag{2.18}$$

$$\ddot{q} + \varepsilon(q^2 - 1)\dot{q} + q = f \tag{2.19}$$

$$\delta = \omega_0/\omega_s = \frac{1}{StU_r} \tag{2.20}$$

$$U_r = \frac{2\pi U}{\omega_0 D} \tag{2.21}$$

Examine now the coupling between these two equations, represented by the forcing term in each. To keep the model relatively simple, only linear terms will be considered in the coupling terms. The forcing of equation 2.14, S, is related to the fluctuating lift coefficient by

$$S = \frac{1}{2}\rho U^2 D C_L. \tag{2.22}$$

Non-dimensinalizing gives the expression for the forcing term in equation 2.18,

$$s' = Mq \tag{2.23}$$

$$M = \frac{C_{L,0}}{2}\frac{1}{8\pi^2 St^2 \mu} \tag{2.24}$$

Since M is a function of the mass ratio, it scales the effect of the wake on the structure. An expression for the forcing term in the wake equation can now be formulated. Since three different kinds of coupling will be studied here, and there is little theoretical justification for them, we'll begin with the non-dimensional form directly. The displacement, velocity, and acceleration coupling terms, respectively, will have a tunable coefficient used to match the model with specific characteristics of the CFD results. The three expressions for the forcing are given by

$$f = A_a y \qquad f = A_b \dot{y} \qquad f = A_c \ddot{y}. \tag{2.25a,b,c}$$

Acceleration coupling does an excellent job of qualitatively and quantitatively capturing most of the features of vortex-induced vibration studied in this thesis. It will be seen that by tuning some of the parameters of the equations, the structural time series of the CFD results closely match the results of this model. The acceleration coupling also exhibits the correct hysteresis behavior at the beginning and end of lock-in as well as the correct range of lock-in. A comparison using the Skop-Griffin parameter will again show the high quality of this model using acceleration coupling, especially compared with the other types of coupling proposed here. It will ultimately be shown that this model, using acceleration coupling, is one of the best reduced order models considered.

The parameters of equations 2.18 and 2.19 must be defined, and then results can be compared with those of simulation. Since there is no structural damping in the CFD results, $\zeta = 0$. From Facchinetti, $\gamma = 0.8$; to match the CFD model the ratio of the structural mass to the fluid mass is 10; i.e. $\mu = 10$. Equation 2.23 defines *s,*' and equation 2.24 can be simplified

and approximated as $M = \frac{0.05}{\mu}$. Since the region of interest is lock-in, where the fluid frequency is equal to the natural frequency of the structure, $\delta = 1$. Equation 2.19 only has two parameters, ε and $A_{a,b,c}$, and are used as tuning parameters to match the simulation results. $A_{a,b,c}$ comes from defining f as equation 2.25 and is one of three coefficients, one for each of the three different kinds of coupling. Each of the three couplings defined in equation 2.25 will be used, and the parameters ε and $A_{a,b,c}$ will be tuned in each case to try to match CFD results.

The first to be considered is displacement coupling, equation 2.25a. This coupling seems to fail in almost all aspects of replicating the CFD results. Tuning the parameters ε and A_a results in $\varepsilon = 0.3$ and $A_a = 1$; this coupling vastly underestimates the steady state displacement. Figure 2.6 shows the structural displacement for this coupling and the CFD model. The displacement coupling, with steady state amplitude of 0.1, is not able to match the CFD model, with steady state amplitude of 0.5. It is expected that the other results from this model will also not be able to match the CFD results quantitatively or qualitatively.

The lift coefficient for the displacement model can be observed in Figure 2.7. It is seen that these results are actually closer than the cylinder displacement results. Even though the lift coefficient is not far off from the CFD model, this does not validate this model because the lift and cylinder motion should be closely related; since the cylinder motion is far removed from the CFD results, the closeness of the lift coefficients seems arbitrary.

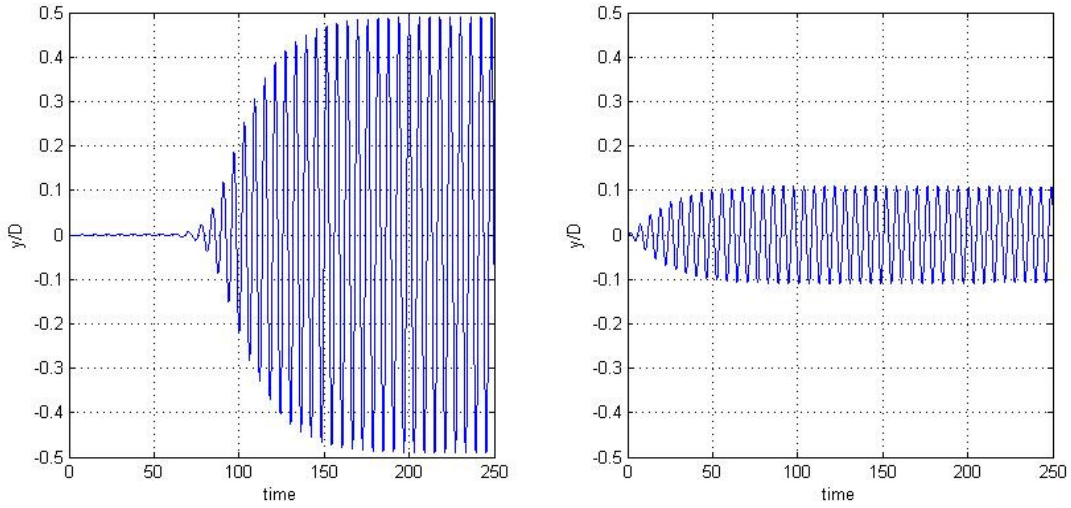

(a) CFD model

(b) Facchinetti model (displacement coupling)

Figure 2.6: Non-dimensional cylinder displacement vs. time for CFD model and Facchinetti model with displacement coupling.

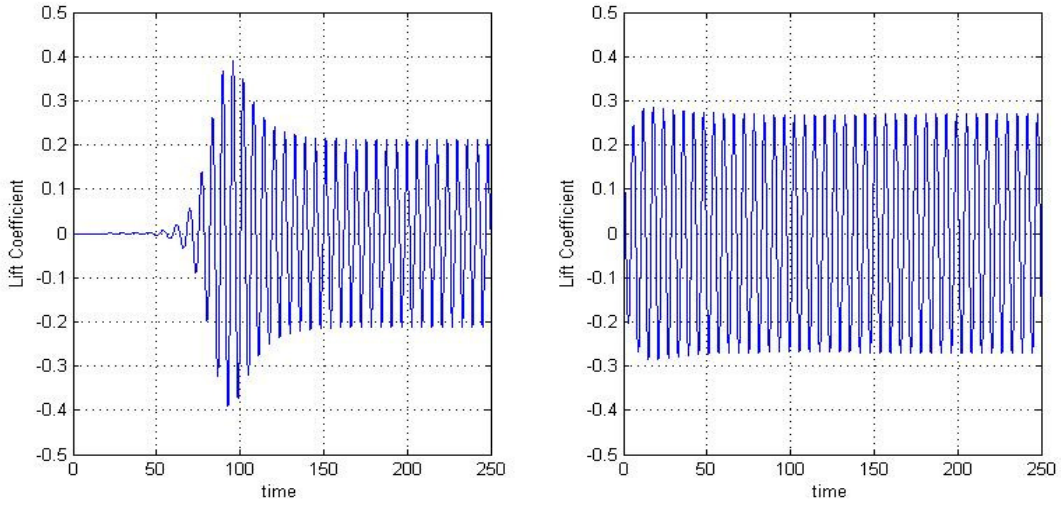

(a) CFD model

(b) Facchinetti model (displacement coupling)

Figure 2.7: Lift coefficient vs. time for CFD model and Facchinetti model with displacement coupling.

The frequency behavior of this model is also inaccurate, as seen in Figure 2.8. The frequency does match the Strouhal frequency outside of lock-in, but entering lock-in seems to

have a small effect on the frequency of this system, as there is a very narrow frequency lock-in region.

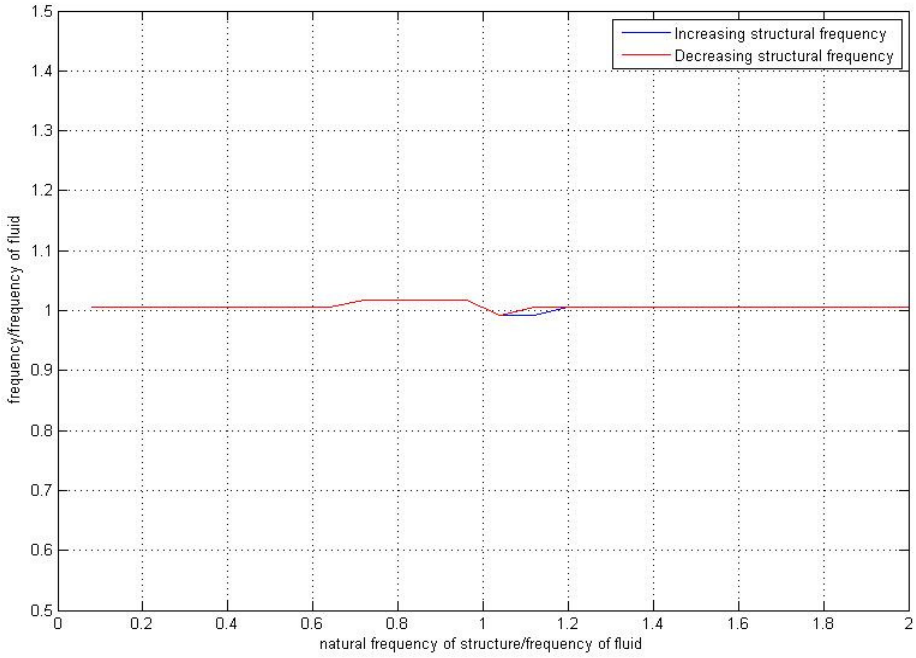

Figure 2.8: The frequency of vibration of the cylinder vs. the natural structural frequency normalized by the frequency of the vortex shedding for the Facchinetti model (displacement coupling).

The amplitude vs. Reynolds number plots seen in Figure 2.8 also show large deviations between this model and the CFD model. There is amplitude amplification which defines a region of lock-in, but the amplitude underestimates the CFD amplitude throughout this region, and the range of lock-in is smaller in the displacement coupling model compared with the CFD model.

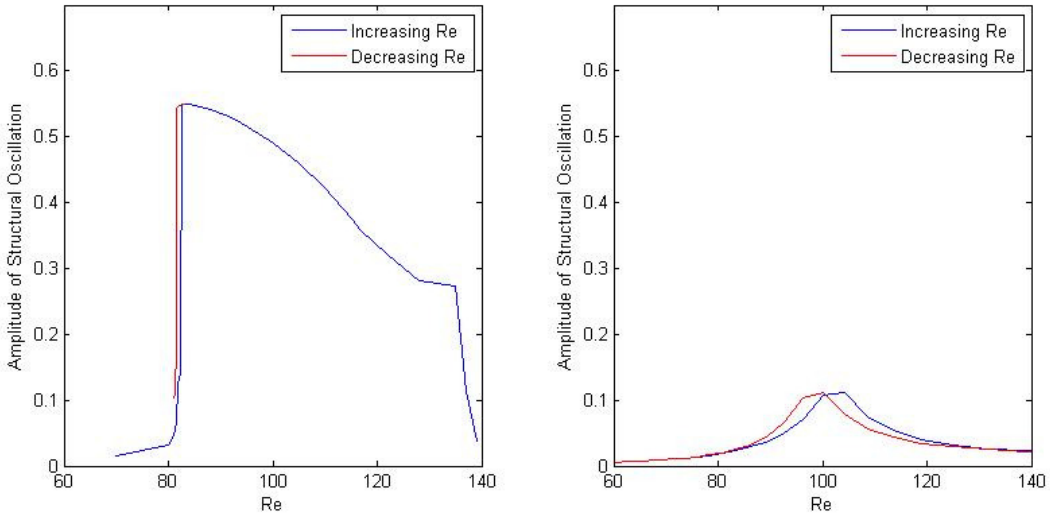

(a) CFD model

(b) Facchinetti model (displacement coupling)

Figure 2.9: The steady-state structural amplitude vs. Reynolds number for increasing and decreasing Reynolds number.

The last plot to consider for the displacement coupling is the Griffin plot seen in Figure 2.10. As expected, the amplitude is underestimated in this model for a range of Skop-Griffin parameter values. The CFD model also seems to decrease in amplitude at a faster rate than the displacement coupling model when increasing the damping of the system. Overall, the Facchinetti model with displacement coupling misses on every comparison considered here; thus, it cannot be considered for accurately modeling VIV. This conclusion agrees with that found in Facchinetti (2004).

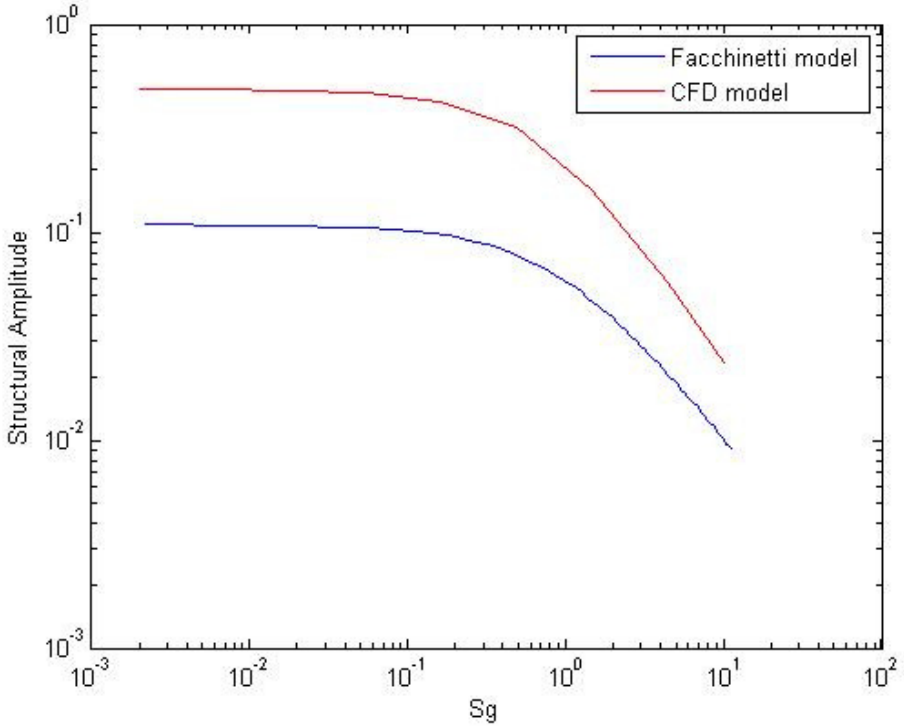

Figure 2.10: Griffin plot for Facchinetti model (displacement coupling) and CFD model.

Next, we consider the velocity coupling, equation 2.25b. This coupling is also unable to capture some of the essential behavior of the CFD model. After tuning ε and A_b in an attempt to match CFD results, the values of the parameters are $\varepsilon = 0.025$ and $A_b = 5.75$. The structural oscillation of this model and the simulation results are shown in Figure 2.11.

This figure shows that the structural amplitude is significantly less for the velocity coupling model compared with the CFD model; thus, it also fails in correctly modeling the cylinder displacement accurately. The lift coefficient is seen below in Figure 2.12. This also differs significantly between the two models as the velocity coupling model greatly overestimates the lift coefficient, while underestimating the structural amplitude.

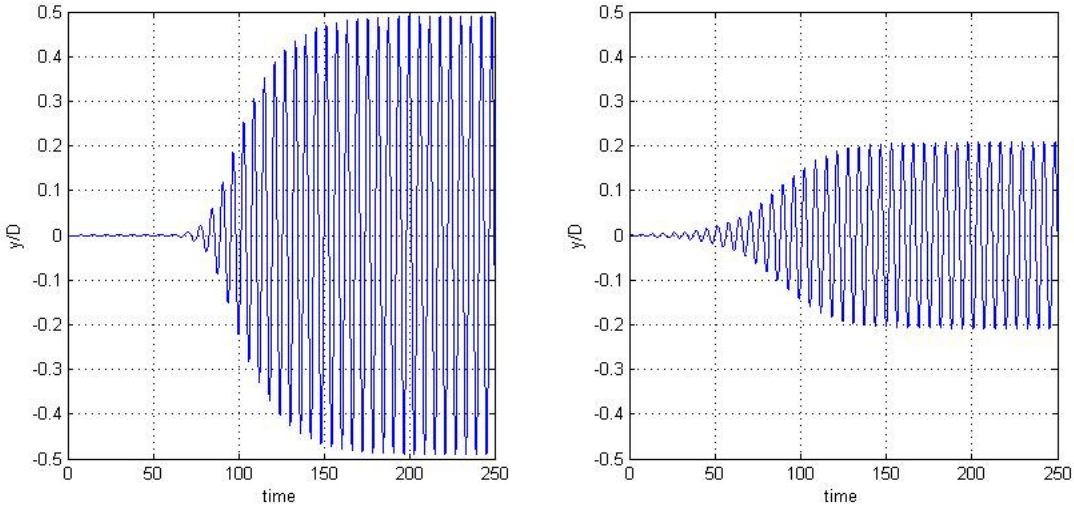

(a) CFD model (b) Facchinetti model (velocity coupling)

Figure 2.11: Non-dimensional cylinder displacement vs. time for CFD model and Facchinetti model with velocity coupling.

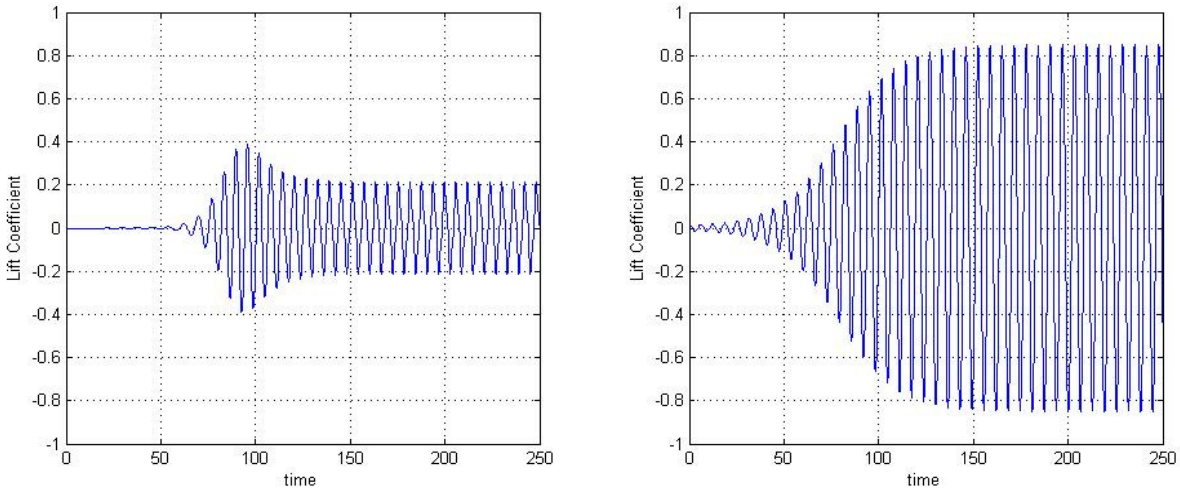

(a) CFD model (b) Facchinetti model (velocity coupling)

Figure 2.12: Lift coefficient vs. time for CFD model and Facchinetti model with velocity coupling.

The frequency response for the velocity coupling model can be seen in Figure 2.13. Before and after lock-in the frequency of vibration is equal to the frequency of the fluid or the Strouhal frequency defined by equation 2.5, and during lock-in the frequency of vibration is near the natural structural frequency. These results are consistent with the CFD model, but

there is also hysteresis only at one end of lock-in which is not consistent. Another look at hysteresis can be found by plotting the structural amplitude vs. *Re*. This plot can be seen in Figure 2.14 and shows that hysteresis only occurs at one end of lock-in and the amplitude is underestimated.

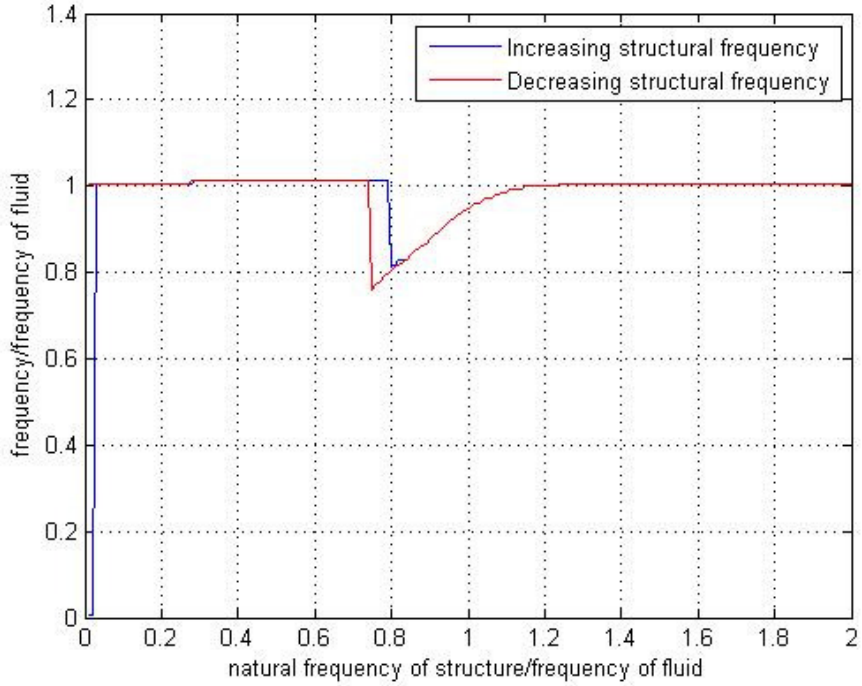

Figure 2.13: The frequency of vibration of the cylinder vs. the natural structural frequency normalized by the frequency of the vortex shedding for the Facchinetti model (velocity coupling).

The final plot to consider is the Griffin plot in Figure 2.15. This plot shows again that the velocity coupling model underestimates the structural amplitude, but it does have the same general shape of the CFD model as they each decrease in amplitude with increasing damping at approximately the same rate.

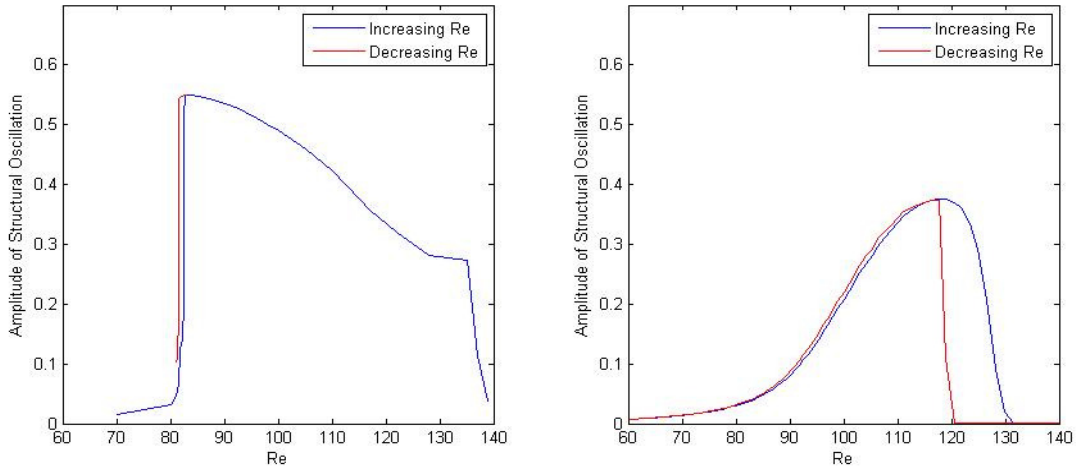

(a) CFD model (b) Facchinetti model (velocity coupling)

Figure 2.14: The steady state structural amplitude vs. Reynolds number for increasing and decreasing Reynolds number.

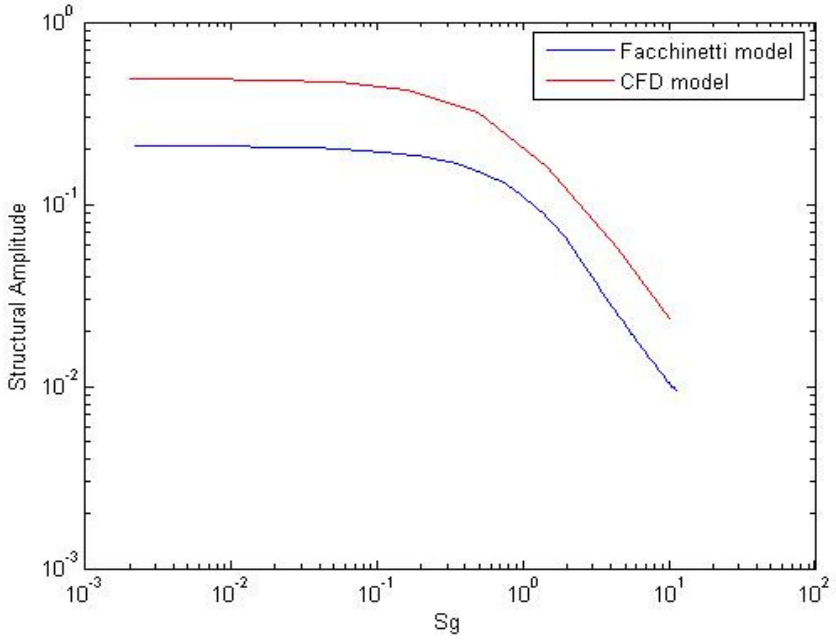

Figure 2.15: Griffin plot for Facchinetti model (velocity coupling) and CFD model.

The final variant to be considered in this model is acceleration coupling, equation 2.25c. This turns out to be the coupling model that best matches the results of the CFD model. The parameters ε and A_c are tuned to best match the CFD results. The final values of the

parameters are ε=0.05 and $A_c = 11.5$. With these values the structural displacement can be seen in Figure 2.16.

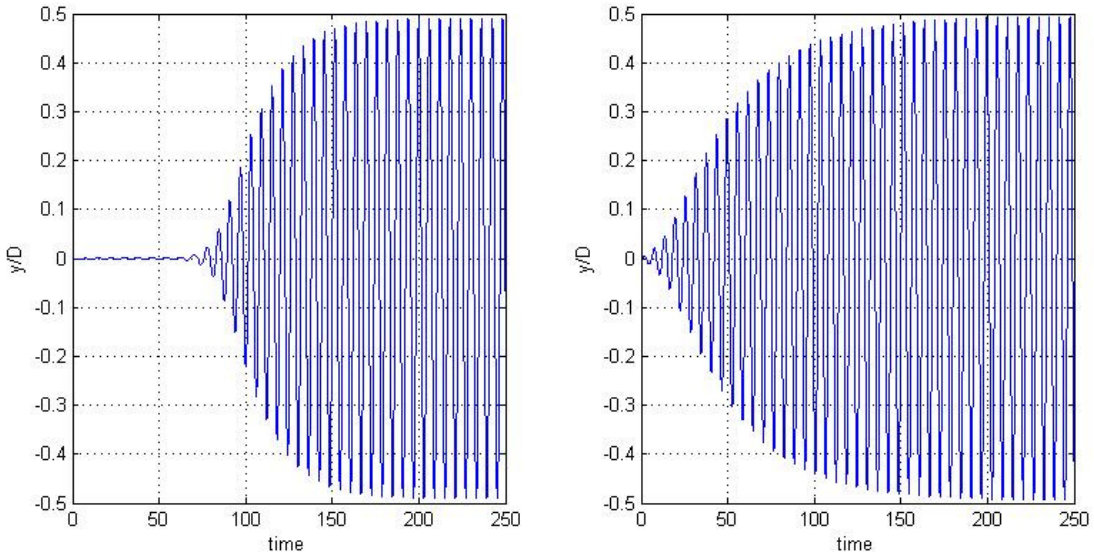

(a) CFD model results

(b) Facchinetti model results (acceleration coupling)

Figure 2.16: Non-dimensional cylinder displacement vs. time for CFD model and Facchinetti model with acceleration coupling.

The structural displacement of the acceleration coupling model matches the CFD results because the parameters were tuned to best fit this data, and this coupling leads to large amplitude amplification, unlike the displacement and velocity coupling models. The shape of each of these plots is also similar, which is promising for indicating that other results will match. The lift coefficient of the model is a direct result of matching the structural displacement; the results can be seen in Figure 2.17. It is clear from these plots that the steady state amplitude of the lift coefficient using the acceleration coupling model differs significantly from the CFD results. The CFD results show a steady-state amplitude around 0.2 while the Facchinetti results show a steady-state amplitude around 1.16. This difference, although large, does not appear to be arbitrary. A plot of the lift coefficient vs. Reynolds number shows that as the CFD model

enters lock-in the lift coefficient tends toward a very high value, near 1.16, but then decreases throughout the lock-in region, ending up at a value of 0.2 when the strouhal frequency exactly matches the natural structural frequency, which occurs at *Re*=100. The plot of lift coefficient vs. Reynolds number can be seen in Figure 2.18.

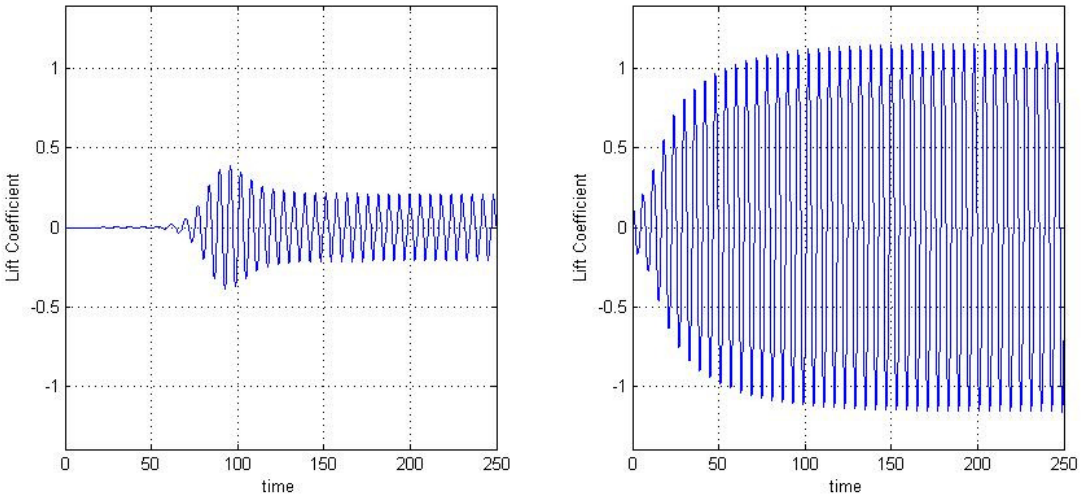

(a) CFD model results

(b) Facchinetti model results (acceleration coupling)

Figure 2.17: Lift coefficient vs. time for CFD model and Facchinetti model with acceleration coupling.

As Figure 2.18 shows the maximum values of the lift coefficients over the lock-in regime are similar for the CFD model and the acceleration coupling model; however, while the acceleration coupling model's lift coefficient stays approximately constant throughout lock-in, the CFD model's lift coefficient decreases throughout lock-in. The inability of the Facchinetti model to capture this behavior is a disadvantage of the model.

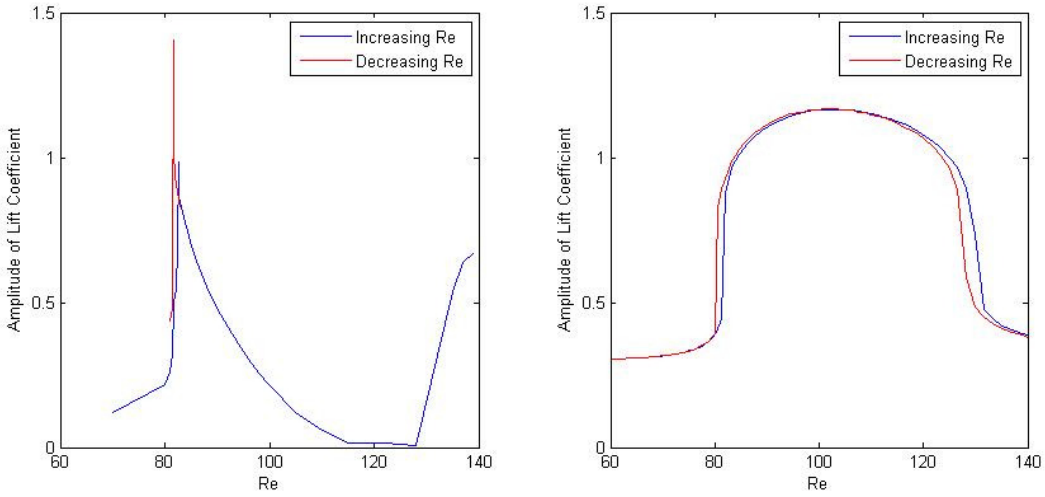

(a) CFD model

(b) Facchinetti model (acceleration coupling)

Figure 2.18: Lift coefficient vs. Re for CFD model and Facchinetti model with acceleration coupling.

The frequency effects of the Facchinetti model closely resemble those of the CFD model. Figure 2.19 shows how the frequency of vibration changes before, during, and after lock-in. This plot illustrates that before and after lock-in the frequency is close to the Strouhal frequency, which is consistent with known results for VIV. During lock-in the frequency of vibration locks onto the natural structural frequency exactly, which corresponds to the results of the CFD model which also shows frequency lock-in. This frequency behavior is a major advantage over the Krenk and Nielsen model.

The amplitude vs. *Re* plot for the acceleration coupling model shows behavior similar to the CFD model. In Figure 2.20 shows we see that results of both CFD and acceleration coupling models show hysteresis at the beginning and end of lock-in. They also show a similar range of lock-in, beginning at *Re*=80 and ending around *Re*=135. The amplitude magnification also matches, though this is expected since the parameters are tuned so the amplitudes of

structural oscillation match. This structural amplitude vs. *Re* plot shows the advantage of the acceleration coupling model over other coupling models in the Facchinetti model as well as the Krenk and Nielsen model.

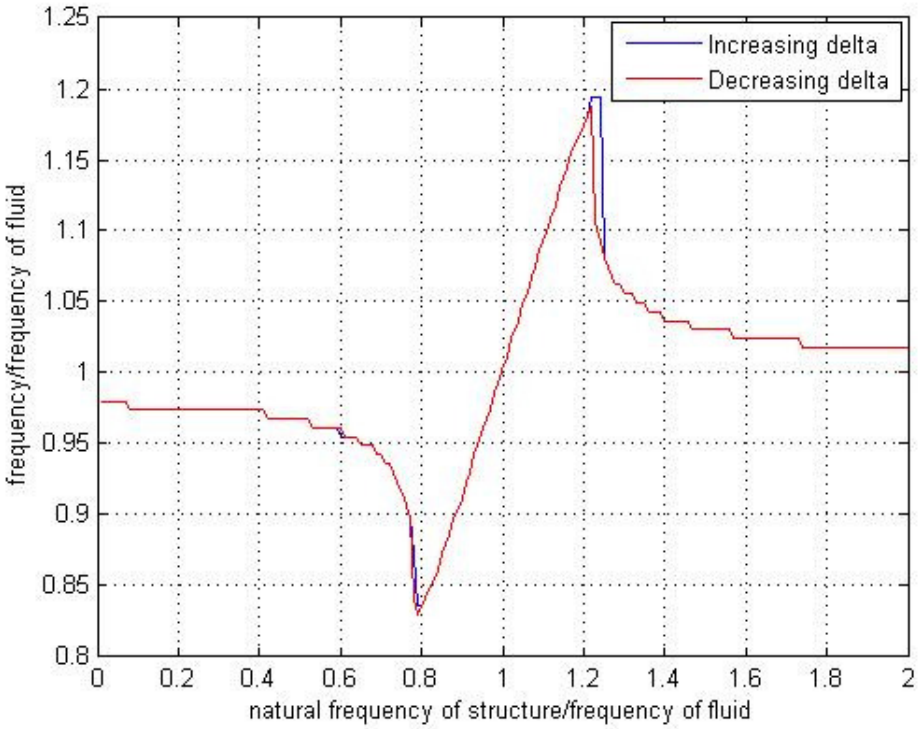

Figure 2.19: The frequency of vibration of the cylinder vs. the natural structural frequency normalized by the frequency of the vortex shedding for the Facchinetti model (acceleration coupling).

The Griffin plot of the Facchinetti model with acceleration coupling also matches well with the CFD model when compared with the other reduced-order models, and Figure 2.21 shows this. The two models start at the same amplitude at low damping, and as the damping is increased the acceleration coupling model decreases at a slightly higher rate than the CFD model, but is significantly better than the other models considered.

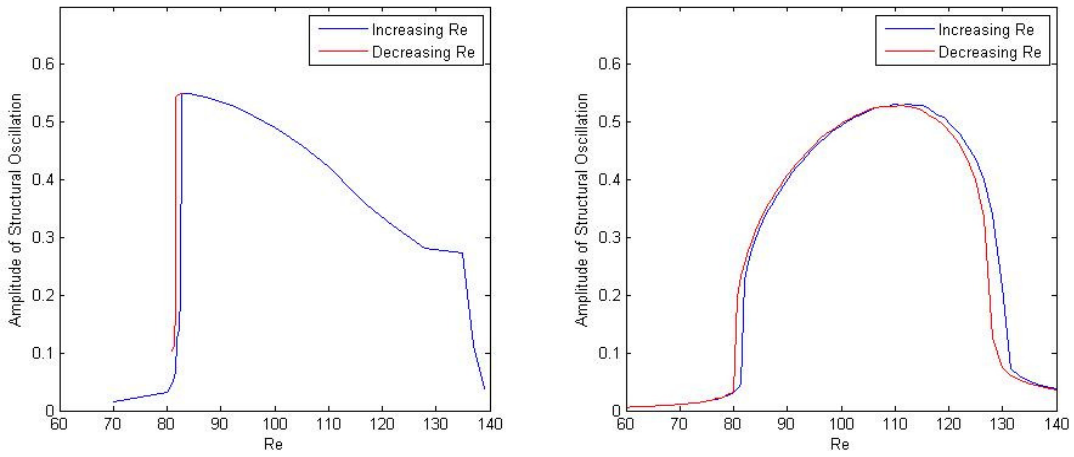

(a) CFD model

(b) Facchinetti model (acceleration coupling)

Figure 2.20: The steady-state structural amplitude vs. Reynolds number for increasing and decreasing Reynolds number.

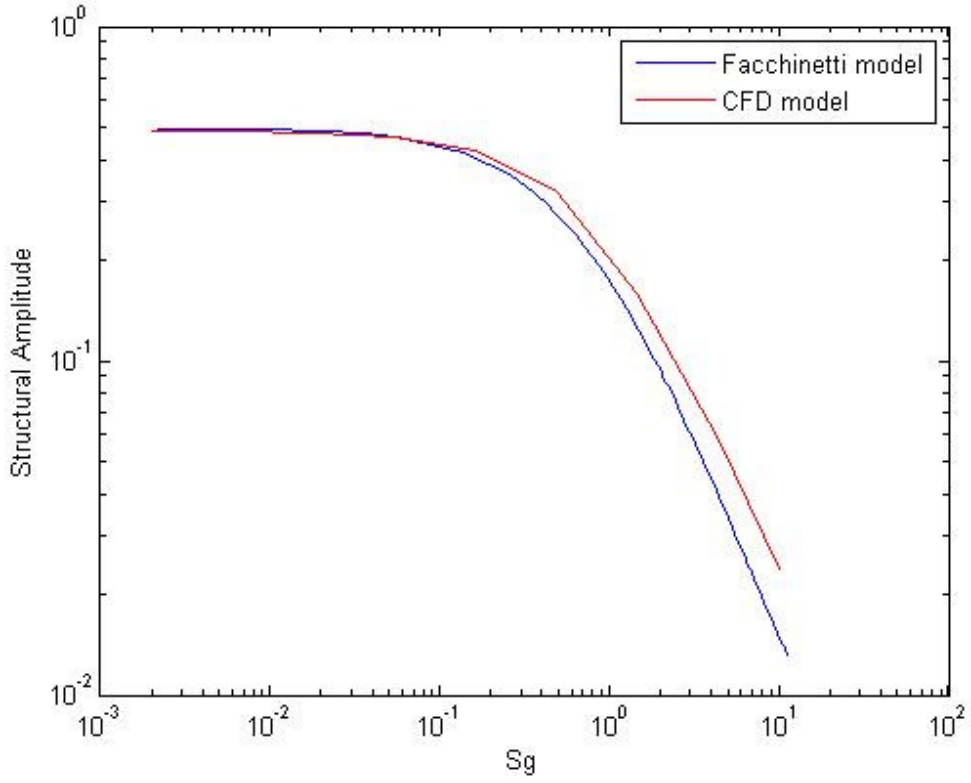

Figure 2.21: Griffin plot for Facchinetti model (acceleration coupling) and CFD model.

2.4 Lin Model

The model by Lin, Ling, Wu, and Zeng (2009) assumes a form very similar to that of Facchinetti. There is one major difference between the two: that is, that the Lin model uses nonlinear fluid damping in the structural oscillator while the Facchinetti model uses a linear term. The non-dimensional equations that describe the Lin model are

$$\ddot{y} + \left(2\zeta\delta + \frac{C_D}{2\mu}|\dot{y}|\right)\dot{y} + \delta^2 y = Mq \tag{2.26}$$

$$\ddot{q} + \varepsilon(q^2 - 1)\dot{q} + q = A\ddot{y} \tag{2.27}$$

where C_D, the drag coefficient, is assumed to be constant, and the expressions for the coupling are already substituted into the equations. As equation 2.27 shows, acceleration coupling is assumed based on the Facchinetti model. Comparing equations 2.18 and 2.26 shows several differences between the structural oscillator of this model and that of the Facchinetti model. A $\frac{C_D}{2}$ term is used in 2.26 in place of the γ term used in 2.18, but this difference is not significant since both terms are taken to be constant. The major difference between these models is the inclusion of a structural velocity term in the fluid damping of equation 2.26. This term makes the structural oscillator nonlinear, while in the Facchinetti model the structure is modeled as a linear oscillator. The addition of the nonlinear fluid damping term is meant to help accurately capture the amplitude of the structural vibrations. In Facchinetti (2004), values of *A*=12 and ε=0.3 are found and used throughout, and adopted by Lin. With these values the model by Facchinetti does underestimate experimental results of the amplitude of the structural vibrations, while the Lin model predicts higher amplitude. In this study, the parameters *A* and ε are tuned to match simulation results so the nonlinear fluid damping term may not be very

significant when modeling the structure, but could play a role in producing different lift coefficient results.

The equations for this model are given in equations 2.26 and 2.27; the parameters must be defined before results can be compared with CFD results. In equation 2.26, $\delta = 1$ since lock-in is the area of interest, and $\zeta = 0$ since there is no structural damping in the simulations. From Lin, the drag coefficient is assumed to be constant, $C_D = 2$; the CFD model uses a mass ratio of 10, so $\mu = 10$ and $M = \frac{0.05}{\mu}$, the same as in Facchinetti. In equation 2.27, the parameters A and ε are tunable, adjusted to match the CFD structural displacement results, giving $A = 4.5$ and $\varepsilon = 0.175$.

The structural response of this model can be seen in Figure 2.22; since the model parameters are tuned to data, its steady-state amplitude matches the CFD model.

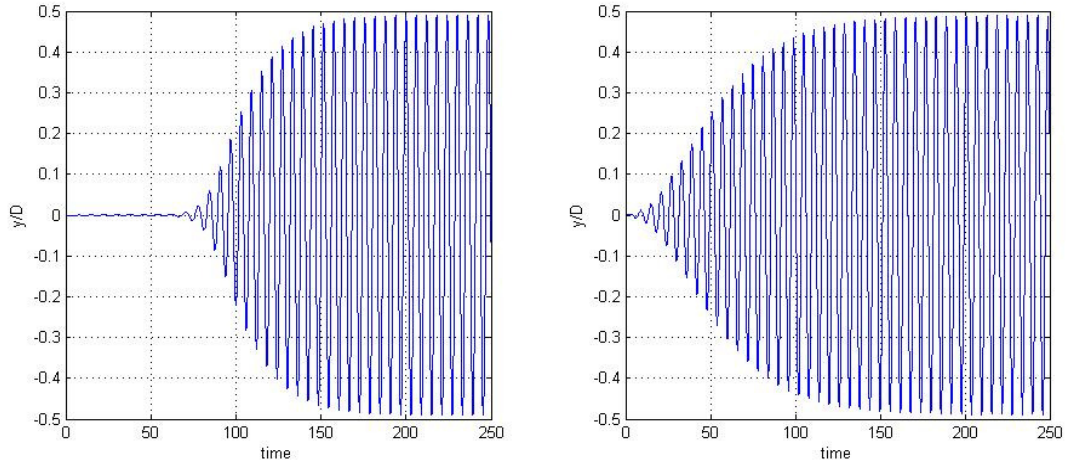

(a) CFD model (b) Lin model

Figure 2.22: Non-dimensional cylinder displacement vs. time for CFD model and Lin model.

Once the structural displacement is matched, as seen in Figure 2.22, the lift coefficient time series is determined. As seen in Figure 2.23, the steady-state lift coefficient is about three times

too large in the Lin model when compared with the CFD model. Just as with the Facchinetti model, a solution to this will be sought by plotting the lift coefficient vs. the Reynolds number over the range of lock-in. This plot can be seen in Figure 2.24. The correct hysteresis behavior is seen in the Lin model but, like the Facchinetti model, the lift coefficient in the Lin model stays constant throughout the lock-in region (Figure 2.24b) while in the CFD model the lift coefficient decreases throughout the same region (Figure 2.24a). Unlike the Facchinetti model, where the lift coefficient seemed to lock onto the initial lift coefficient at lock-in of the CFD model, the Lin model locks onto a value of 0.6, this is between the initial lock-in value and the value at *Re*=100.

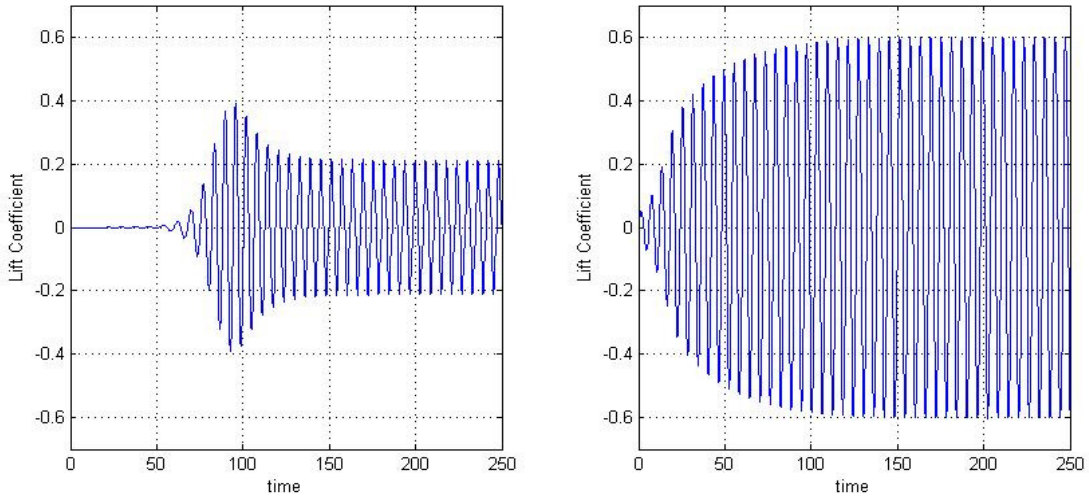

(a) CFD model (b) Lin model

Figure 2.23: Lift coefficient vs. time for CFD model and Lin model.

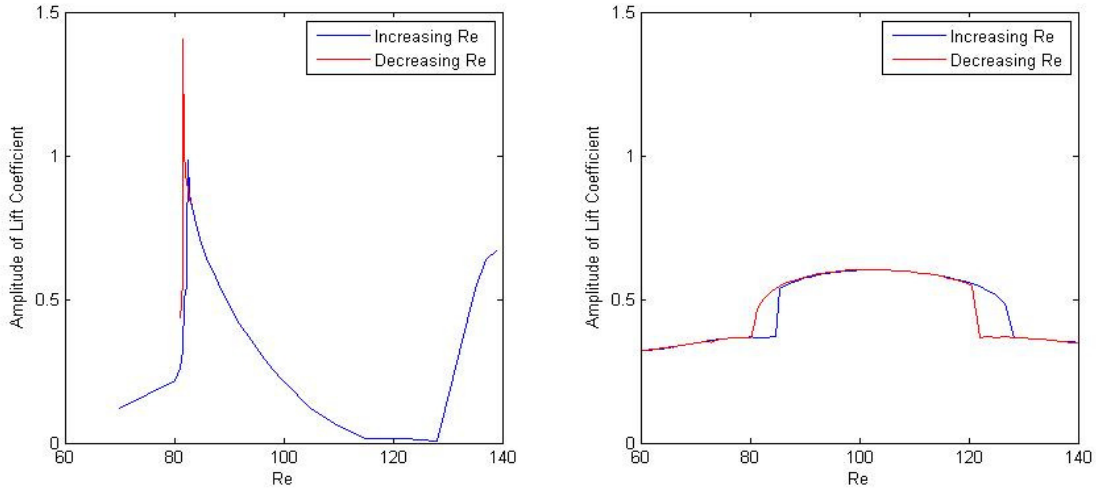

(a) CFD model (b) Lin model

Figure 2.24: Lift coefficient vs. Re for CFD model and Lin model.

The frequency of the vibration vs. the natural frequency of the structure is normalized by the fluid frequency and plotted in Figure 2.25. It can be seen that before lock-in the frequency of vibration matches the frequency of the fluid, or the Strouhal frequency. Once lock-in is reached the frequency of vibration jumps to the natural frequency of the structure and stays there throughout lock-in, and after lock-in the frequency returns to the Strouhal frequency. This behavior is correct, but the range of lock-in does not correspond to the range seen in Figures 2.24 and 2.26. The range of lock-in in Figure 2.25 corresponds to Reynolds numbers that range from about 50 to 200 which is significantly larger than the range of Reynolds numbers for lock-in seen in Figures 2.24 and 2.26, which is about 80 to 125. When comparing this to the Facchinetti model with acceleration coupling, the Facchinetti model does a much better job at lock-in, matching the region of amplitude amplification, as seen in Figures 2.19 and 2.20.

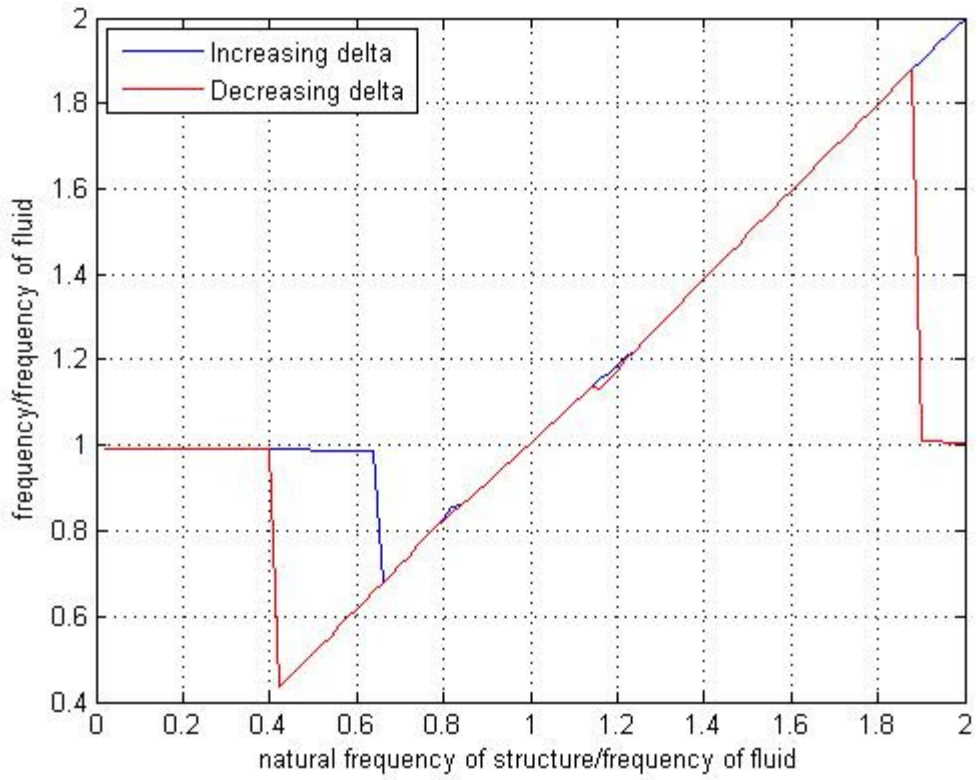

Figure 2.25: The frequency of vibration of the cylinder vs. the natural structural frequency normalized by the frequency of the vortex shedding for the Lin model.

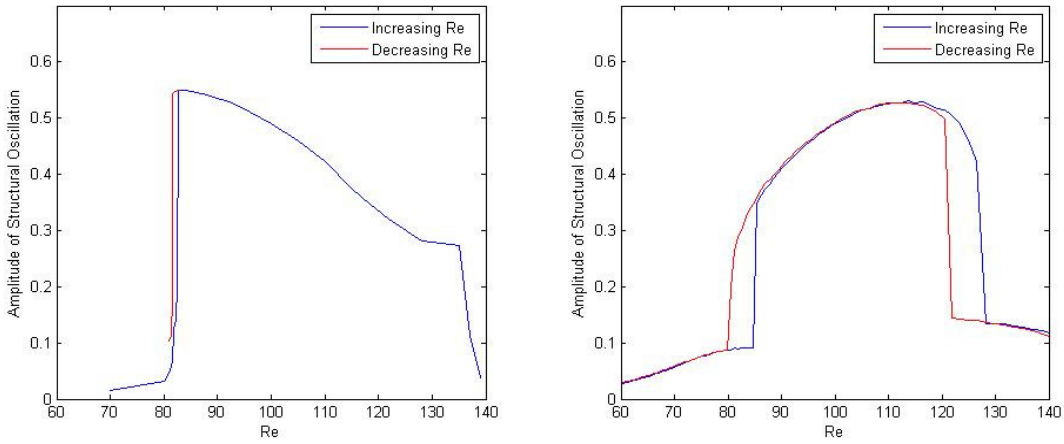

(a) CFD model (b) Lin model

Figure 2.26: The steady state structural amplitude vs. Reynolds number for increasing and decreasing Reynolds number for the Lin model.

Figure 2.26 shows the amplitude of the structural oscillation though the lock-in regime. The amplitude of the Lin model matches the amplitude of the CFD model, but the range of lock-in is slightly smaller in the Lin model. Hysteresis is also seen at the beginning and end of lock-in for both the Lin model and CFD model, but the range of hysteresis is larger for the Lin model. When comparing these results with the Facchinetti model with acceleration coupling, it appears that the Facchinetti model does a better job of matching the CFD results.

The Griffin plot for the Lin model can be seen in Figure 2.27 showing how the structural amplitude changes with the Skop-Griffin parameter, related to structural damping.

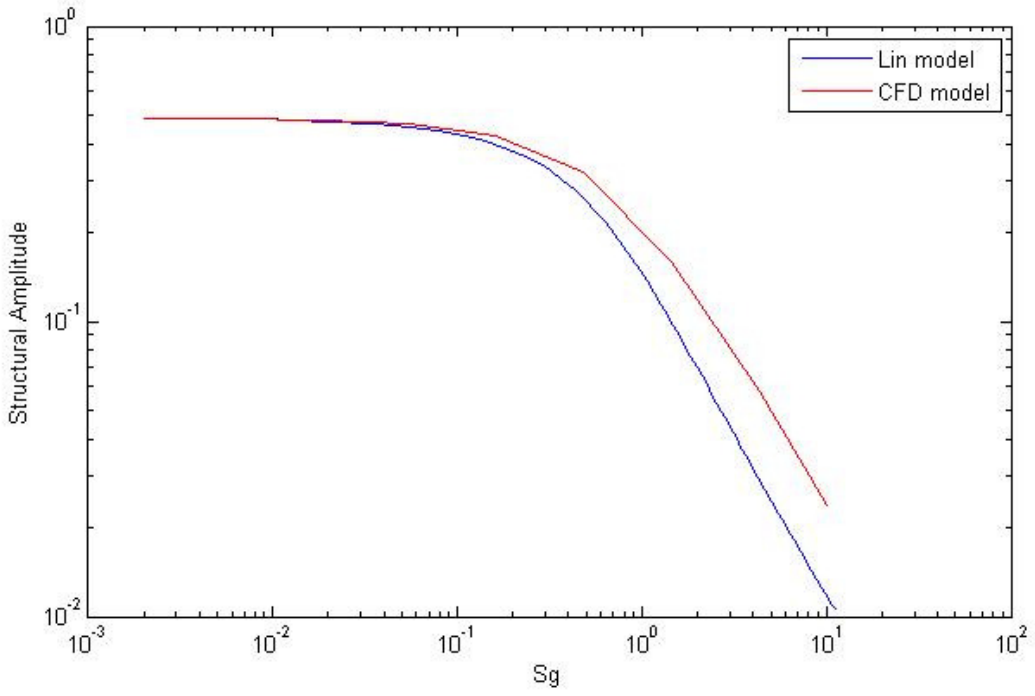

Figure 2.27: Griffin plot for Facchinetti model (acceleration coupling) and CFD model.

The Lin model does a good job of matching the CFD results, especially at low structural damping. Both of these models also start to decrease in amplitude around the same value of the Skop-Griffin parameter, but the Lin model appears to decrease in amplitude faster than the

CFD model. The Lin model results are very similar to the Facchinetti model with acceleration coupling seen in Figure 2.21, but the Facchinetti results resemble the CFD results more closely.

2.5 Farshidianfar and Zanganeh Model

This model, by Farshidianfar and Zanganeh (2010), introduces a new structural oscillator, in the form of a van der Pol oscillator. The idea behind this is to capture the system behavior at both high and low mass damping ratios. In trying to accurately model VIV, it is believed that small oscillations feed energy into the system and large oscillations remove it. In other engineering disciplines such as electrical engineering, biochemistry, and optical physics, systems with these characteristics are common. These systems are often modeled by two coupled van der Pol oscillators, and this is adopted here to model VIV.

Consistent with the Facchinetti model, three different forms of coupling can be considered: displacement, velocity, and acceleration. The equations of motion for this model are

$$\ddot{y} + \varepsilon\left(2\zeta\delta + \frac{\gamma}{\mu}\right)(y^2 - 1)\dot{y} + \delta^2 y = Mq \tag{2.28}$$

$$\ddot{q} + \varepsilon(q^2 - 1)\dot{q} + q = f \tag{2.29}$$

where f can be either (2.25a), (2.25b), or (2.25c). The only difference between this model and the Facchinetti model is the adoption of the van der Pol type oscillator as the structural equation; thus, all parameters are defined as they were in Facchinetti (2004).

The primary advantage of this model, according to Farshidianfar and Zanganeh, is its ability to predict VIV results at high and low mass damping ratios. They claim that this is not accomplished in models that use a linear oscillator as the structural equation. A disadvantage of

this model is that, at a flow rate of zero, it predicts self-sustained structural oscillations, which is not physical. Due to this non-physical behavior, it will be seen that this model does not replicate CFD results accurately.

Equations 2.28 and 2.29 describe this model; consistent with the Facchinetti model, $\zeta = 0,\ \delta = 1,\ \gamma = 0.8,\ \mu = 10$and $M = \frac{0.05}{\mu}$. The coupling term, f, in the wake oscillator equation is taken to be equation 2.25b, which is velocity coupling as recommended by Farshidianfar and Zanganeh. It will be shown that using a van der Pol oscillator to represent the structure produces poor results independent of the coupling mechanism. The parameters A and ε, which are tuned to match the CFD results, do not affect the quality of this model significantly; because of this they are taken to be $A = 10$ and $\varepsilon = 0.5$.

The structural response of this model can be seen in Figure 2.28. It can be seen that it differs significantly from the simulation results. Reflecting on the choice of a van der Pol oscillator to represent the structure, the steady-state amplitude is constant for a wide range of parameter values. This makes it difficult to tune the model to match the CFD results. Since the structural amplitude is inaccurate, the lift coefficient is as well, as seen in Figure 2.29. It is interesting to note that the shape of these plots is unique when compared with the CFD results and other models. The unique way in which these results reach steady-state is a result of the behavior of the two coupled van der Pol oscillators.

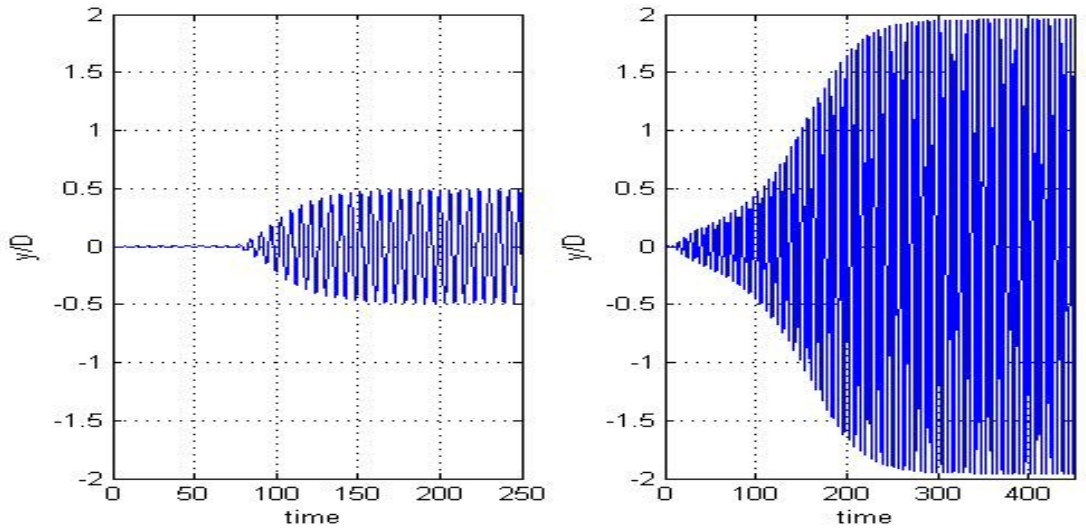

(a) CFD model

(b) Farshidianfar and Zanganeh model

Figure 2.28: Non-dimensional cylinder displacement vs. time for CFD model and Farshidianfar and Zanganeh model.

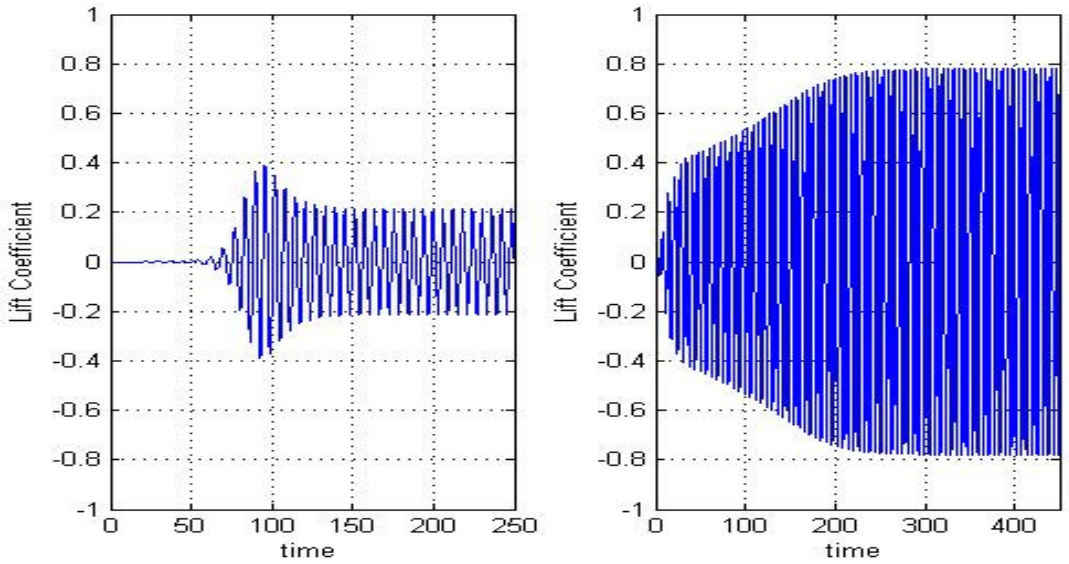

(b) CFD model

(b) Farshidianfar and Zanganeh model

Figure 2.29: Lift coefficient vs. time for CFD model and Farshidianfar and Zanganeh model.

The frequency response of this model can be seen in Figure 2.30. The system shows no sign of frequency lock-in when the vortex shedding frequency approaches the natural frequency of the structure. The frequency of vibration stays locked onto the Strouhal frequency throughout the entire domain despite the fact that in VIV the frequency jumps to the natural frequency of the structure during lock-in. There is also no hysteresis seen in Figure 2.30.

The plot of steady-state amplitude versus Reynolds number is shown in Figure 2.31 where it is again seen that this model does a very poor job of modeling the CFD results. No lock-in region is observed around Re=100, as the amplitude seems to remain constant beyond Re=90. There is actually amplitude amplification beyond y/D=2 before the frequencies match which is not consistent with the CFD model or any known VIV results. This model also significantly overestimates the amplitude of the cylinder throughout the entire range of Reynolds numbers.

The final plot to consider is the Griffin plot of this model compared to the CFD model. Figure 2.32 demonstrates that this model does not match the CFD model at all. Regardless of the value of the Skop-Griffin parameter, the structural amplitude appears to be approximately 2 and this means that, regardless of the damping, the structural amplitude does not change, which is not physical.

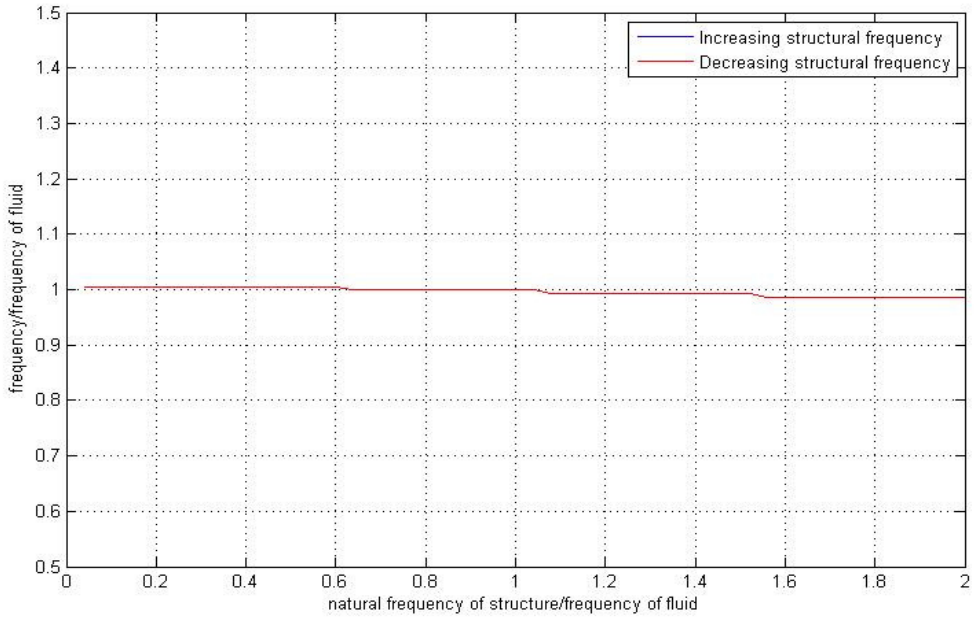

Figure 2.30: The frequency of vibration of the cylinder vs. the natural structural frequency normalized by the frequency of the vortex shedding for the Farshidianfar and Zanganeh model.

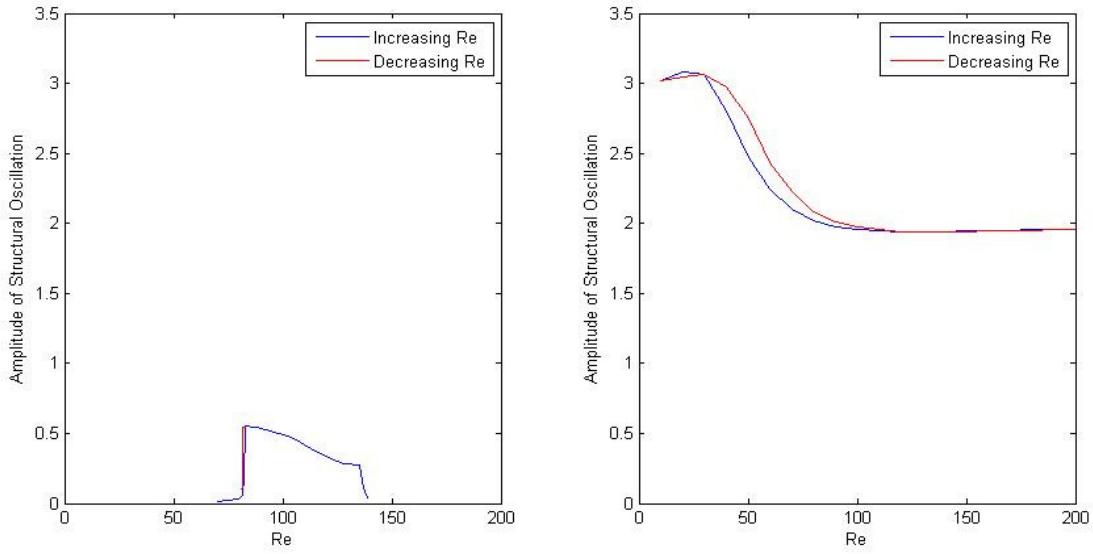

(c) CFD model

(b) Farshidianfar and Zanganeh model

Figure 2.31: The steady-state structural amplitude vs. Reynolds number for increasing and decreasing Reynolds number for the CFD model and the Farshidianfar and Zanganeh model.

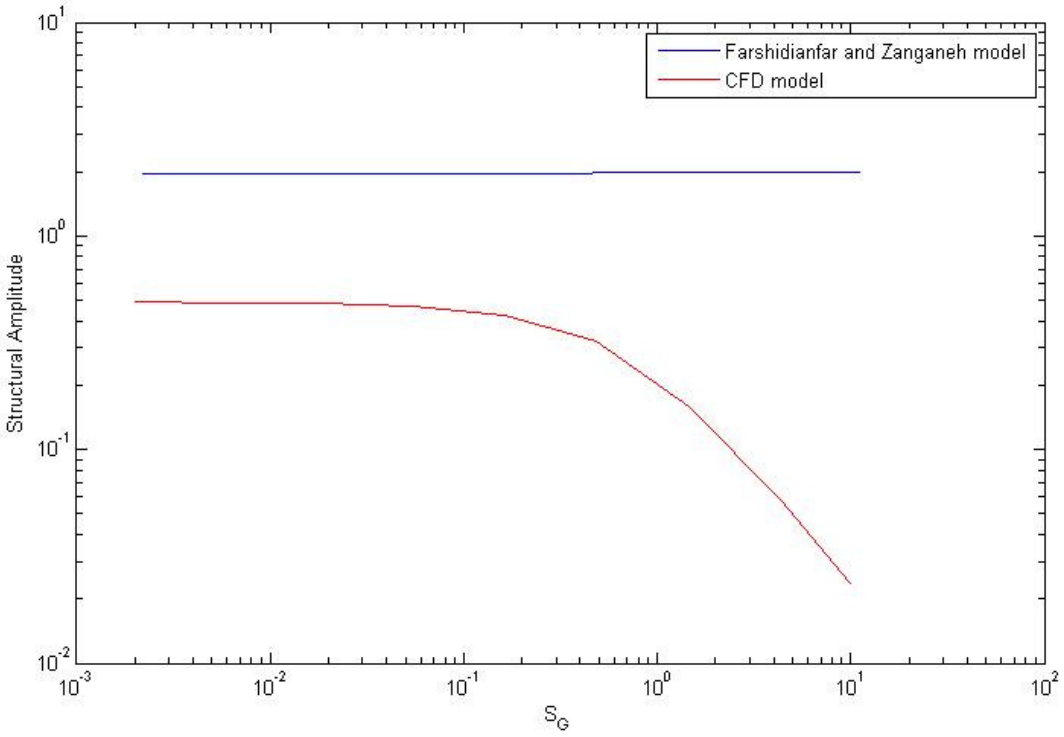

Figure 2.32: Griffin plot for Farshidianfar and Zanganeh model and CFD model.

Chapter 3

Analysis of Results

3.1 General Discussion

As Chapter 2 illustrates, no reduced order model is able to exactly match the CFD results. This is expected since these are approximate models which cannot be expected to capture every detail of the response exhibited by the high fidelity finite element code. By looking at the results for each reduced order model considered, conclusions can be drawn about what aspects of these models accurately reproduce the results of the CFD model. Each model considered has unique characteristics, so they all must be examined in detail.

The Farshidianfar and Zanganeh (2010) model does the worst job of matching the simulation results of all the reduced order models considered. As seen in Figures 2.28 – 2.32, the limit cycle behavior of the structural oscillator prevents this model from accurately modeling VIV. After tuning the parameter, the steady-state structural amplitude remained fixed at 2, typical of the van der Pol oscillator. The amplitude also remains high outside of lock-in even when damping is added to the system. This model fails to exhibit several important VIV phenomena such as frequency lock-in with coincident amplitude amplification. Thus, it can be concluded that this model fails to accurately represent VIV.

The Krenk and Nielsen (1999) model is able to capture many features of VIV seen in the simulation results, but fails in many other ways. It accurately predicts the amplitude of the structural response during lock-in after tuning the parameters, as seen in Figure 2.1. The system

correctly predicts frequency lock-in as the shedding frequency approaches the natural structural frequency. However, as Figure 2.3 shows, the system locks on to a nearby frequency instead of the exact natural frequency of the structure, and it remains at this frequency instead of returning to the Strouhal frequency, again not consistent with VIV results. The lock-in region does exhibit amplitude amplification as seen in Figure 2.4, but it shows two separate modes that each overestimate the maximum structural displacement during lock-in, as opposed to the CFD result which has almost constant amplitude during lock-in and hysteresis at the beginning and end of lock-in. The introduction of damping into the system highlights another discrepancy between this model and simulation results; the amplitude of the simulation results fall off much faster than the Krenk and Nielsen results, as seen in Figure 2.5. From this model it can be concluded that using a non-linear oscillator exhibiting limit cycle behavior as the wake equation with a velocity coupling can model many VIV phenomena, but fails to quantitatively address all of the features seen in the CFD results.

Examining the results from the Facchinetti (2005) model shows that the choice of coupling leads to significant differences in system behavior. Both displacement and velocity coupling fail to accurately reproduce the steady-state structural amplitude, while the acceleration coupling is able to replicate the CFD results better than any other reduced order model considered in this thesis. The acceleration coupling results, seen in Figures 2.16 - 2.21, accurately model the structural displacement after tuning the parameters. The frequency response of this system is also properly modeled as it enters lock-in by jumping to the natural frequency of the structure and eventually exits lock-in as the Strouhal frequency moves away from the structural frequency. The amplitude amplification and range of lock-in is also

accurately portrayed by the acceleration coupling, with hysteresis at the beginning and end of lock-in. The Griffin plot matches the CFD results very closely and is the best match compared to all other reduced order models studied. The one result that is significantly in error is the lift coefficient, as both the time series and lift vs. *Re* differ from the simulation results. This discrepancy can be seen in Figure 2.18; both of these plots show lock-in at approximately the same lift coefficient, but the CFD result exhibits a decreasing lift coefficient throughout lock-in, while the Facchinetti result, along with every other reduced order model, shows a nearly constant lift coefficient throughout lock-in. The inability to model the decreasing lift coefficient throughout lock-in is a consistent flaw in the reduced order models considered here.

The results of the Lin (2009) model, shown in Figures 2.22 – 2.27, resemble those of the Facchinetti model with acceleration coupling quite closely. The difference between them is the introduction a nonlinear fluid damping term in the structural equation of the Lin model. This difference causes a larger area of hysteresis and an extended frequency lock-in region, which does not match the region of amplitude amplification. The lift coefficient behavior is also similar to the Facchinetti model as it remains constant throughout the lock-in region, instead of decreasing throughout like the simulation results. Unlike the Facchinetti model, where the peak lift matched the peak lift of the CFD results, the Lin model has a peak lift that is in between the maximum and minimum values of the CFD results.

From these results, the Facchinetti model with acceleration coupling can be seen to provide the best reduced order model of those studied. The inability of all of these models to replicate the lift coefficient behavior throughout lock-in is a consistent problem; if this could be adjusted in some fashion, more accurate results would be achieved.

3.2 Analysis of Nonlinearity in Wake Equation

From the analysis done on the Facchinetti model, Section 2.3, where three different types of coupling mechanisms were considered, it is seen that acceleration coupling is the most effective. The type of nonlinearity in the wake equation is also of interest, and that will be studied here. It is well known that a limit cycle-type oscillator can be used to model the fluid, but now it will be shown whether a specific one, such as the van der Pol oscillator, should be employed or if a more general nonlinear oscillator with limit cycle behavior is preferable. The Facchinetti model employs a van der Pol oscillator; by replacing this with a more general limit cycle-type oscillator, we can assess whether or not improved performance is obtained.

A combination of van der Pol and Rayleigh oscillators, similar to the nonlinearity used by Krenk and Nielsen (1999), is now going to be employed in the Facchinetti model with acceleration coupling. The system is now given by

$$\ddot{y} + \left(2\zeta\delta + \frac{\gamma}{\mu}\right)\dot{y} + \delta^2 y = Mq \tag{3.1}$$

$$\ddot{q} + \varepsilon(q^2 + \dot{q}^2 - 1)\dot{q} + q = A_c\ddot{y}. \tag{3.2}$$

The parameters are defined the same as in Section 2.3 and have identical values. The tunable parameters ε and A_c are found the same way that they were before, and their final values are, $\varepsilon = 0.012$ and $A_c = 12$. The results of this model can be seen below in Figures 3.1 – 3.6. As these plots show, the results for this modified Facchinetti model match well with the CFD results and closely resemble the results for the original Facchinetti model. The similarity between the model with a van der Pol oscillator and the one with a more general nonlinear oscillator means that, for the purpose of modeling VIV, using a general limit cycle-type oscillator in the wake equation is sufficient.

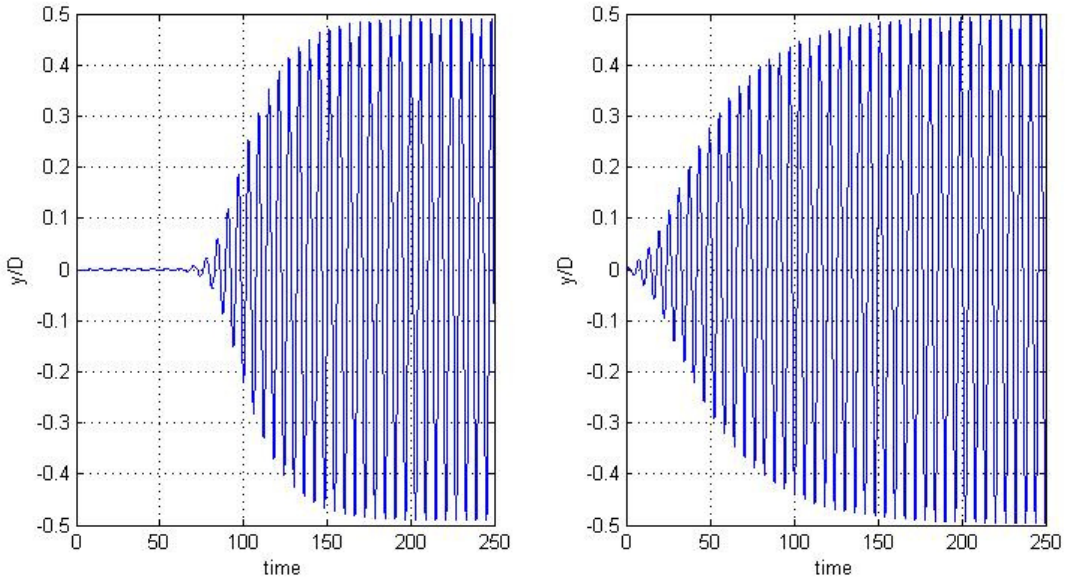

(a) CFD model (b) Modified Facchinetti model

Figure 3.1: Non-dimensional cylinder displacement vs. time for CFD model and modified Facchinetti model.

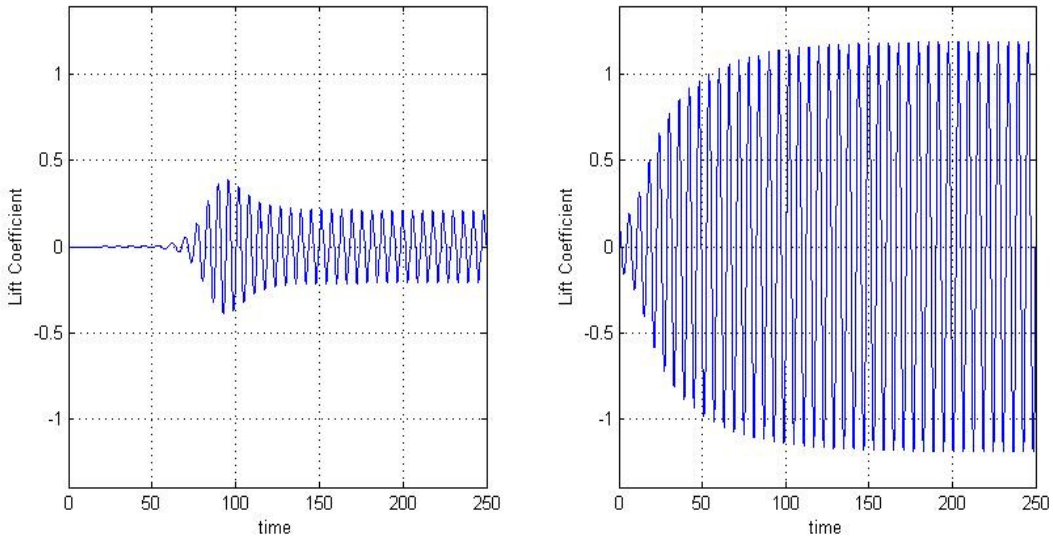

(a) CFD model (b) Modified Facchinetti model

Figure 3.2: Lift coefficient vs. time for CFD model and modified Facchinetti model.

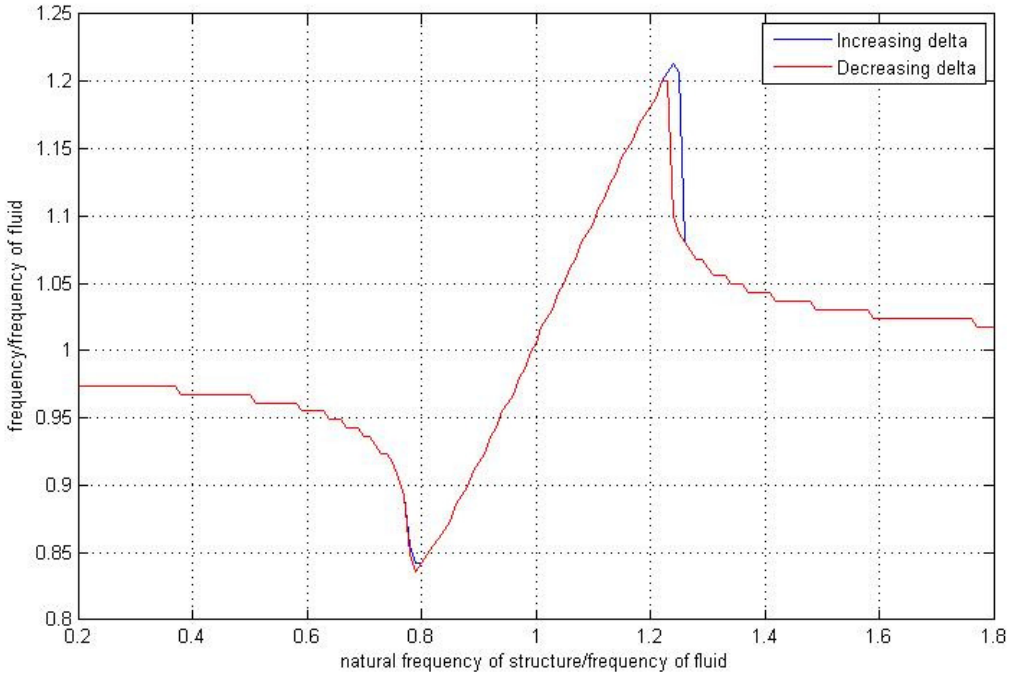

Figure 3.3: The frequency of vibration of the cylinder vs. the natural structural frequency normalized by the frequency of the vortex shedding for the modified Facchinetti model.

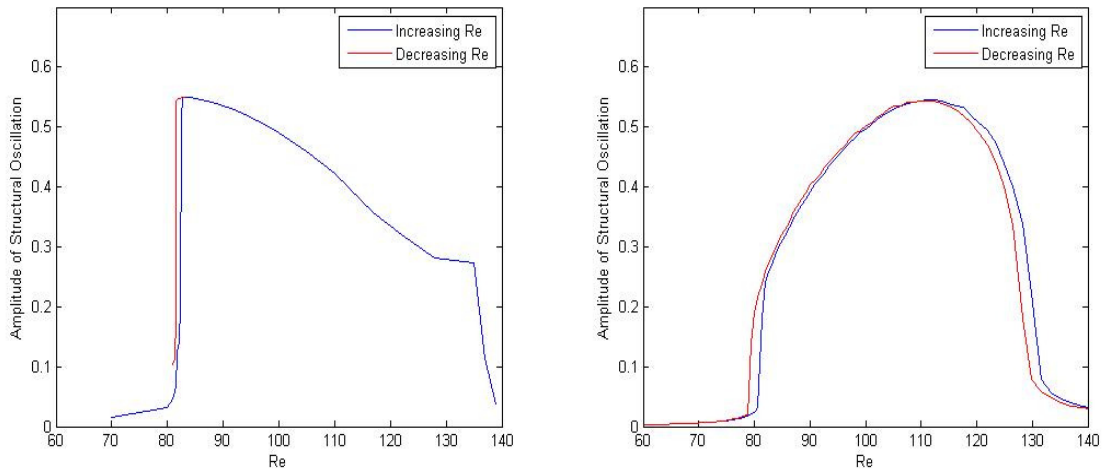

(a) CFD model (b) Modified Facchinetti model

Figure 3.4: The steady-state structural amplitude vs. Reynolds number for increasing and decreasing Reynolds number for the CFD model and modified Facchinetti model.

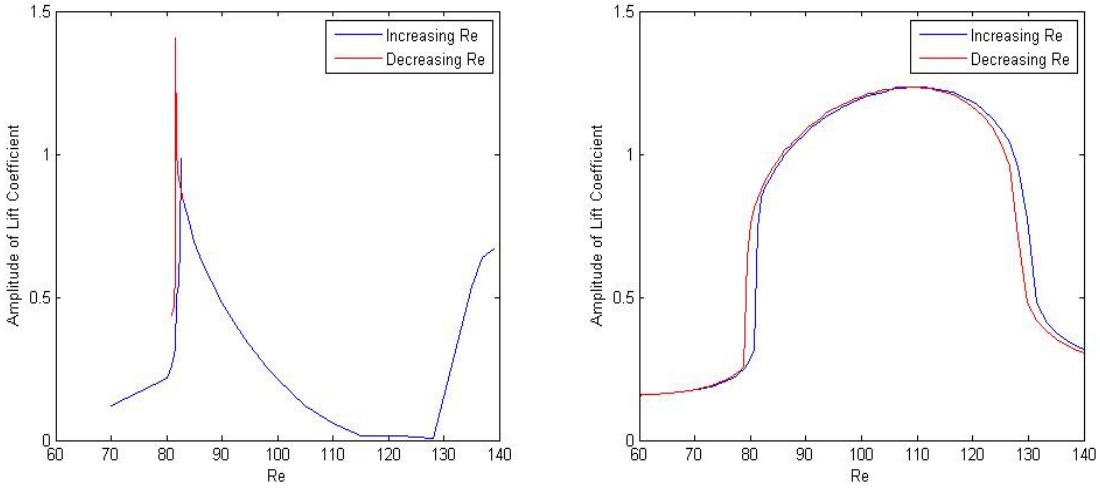

(a) CFD model (b) Modified Facchinetti model

Figure 3.5: The steady-state lift coefficient vs. Reynolds number for increasing and decreasing Reynolds number for the CFD model and modified Facchinetti model.

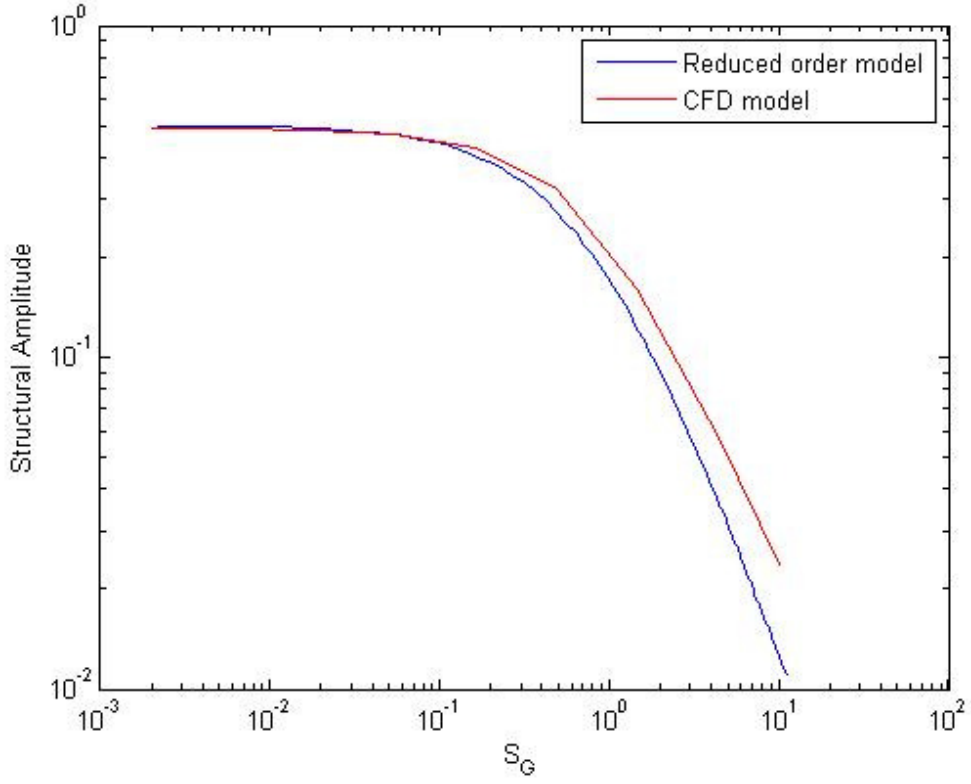

Figure 3.6: Griffin plot for CFD model and modified Facchinetti model.

Chapter 4

Conclusion

4.1 Review of Results

Correctly modeling a system undergoing vortex-induced vibration is an important step when trying to mitigate these vibrations. A high fidelity computational code is one way to completely solve the Navier-Stokes equations coupled to the rigid, sprung cylinder in cross-flow to obtain cylinder response, but this is computationally time consuming and expensive. Using a reduced order model drastically reduces computation time and allows the analyst to obtain an understanding of the physics of the system. The challenge of this approach is to find a simple model that accurately predicts VIV; there are two ways to do this: using data to construct a model or employing ad hoc phenomenological models. The efficacy of the latter was studied in this thesis.

By examining various reduced order models and comparing their responses to CFD results, the strengths and weaknesses of each model were examined to discover what works. The Krenk and Nielsen model predicts some VIV phenomena correctly, but does not quantitatively capture other features seen in the simulation results. The Facchinetti model compares three different kinds of coupling and showed that acceleration coupling works best. Out of all of the reduced order models considered, this one produces the results that most closely resemble those of the CFD model. The Lin model adds nonlinearity to the structural oscillator, but remains similar to the Facchinetti model, with similar results. Farshidianfar and

Zanganeh introduce a van der Pol oscillator into the structural equation, but this leads to poor results since the limit cycle behavior produces non-physical results.

A characteristic that none of the models was able to capture was the lift coefficient behavior throughout lock-in. Figure 2.18 shows this deficiency in the Facchinetti model with acceleration coupling; it too was unable to produce a decreasing lift coefficient throughout lock-in. The peak lift coefficients do match in this plot, but the response of the reduced order model stays approximately constant across lock-in.

The type of nonlinearity in the wake equation is also of interest; this is explored in Section 3.2. In the original Facchinetti model, acceleration coupling and a van der Pol oscillator are used to produce the best results. To see if this nonlinearity is required for good results, a more general limit cycle-type oscillator was employed, and the plots show that this model is sufficient. In conclusion, to produce results that closely match simulations, a linear structural equation coupled to a nonlinear wake equation should be used, where the wake equation exhibits any limit cycle-type nonlinearity and acceleration coupling.

4.2 Future Work

In this thesis, several previously published phenomenological models were examined and compared with a high fidelity finite element model of vortex induced vibration. Some of these models were able to capture many features of the simulation results, but none of them were able to completely match the simulations. Future research is focused on developing a data-driven model which hopefully will be able to capture all VIV phenomena, including the decreasing lift coefficient throughout lock-in. More importantly, a more accurate reduced order

model will provide the means to better understand the physics of VIV. Once VIV is better understood, it will be easier to attempt to suppress vibrations in the system, thus accomplishing the primary goal of this research.

Bibliography

[1] Benaroya H., Gabbai R.D. (2008). Modeling vortex-induced fluid-structure interaction. *Philosophical Transactions of the Royal Society A* 366, 1231-1274.

[2] Birkoff G., Zarantanello E.H. (1957). Jets, Wakes, and Cavities. *Academic Press, New York*.

[3] Bishop R.E.D, Hassan A.Y. (1964). The lift and drag forces on a circular cylinder oscillating in a flowing fluid. *Proceedings of the Royal Society of London A* 277, 51-75.

[4] Calderer, R., Masud, A., (2010). A multiscale stabilized ale formulation for incompressible flows with moving boundaries. *Computational Mechanics* 46, 185–197, 10.1007/s00466-010-0487-z.

[5] Dowell E.H. (1981). Non-linear oscillator models in bluff body aero-elasticity. *Journal of Sound and Vibration* 75(2), 251-264.

[6] Facchinetti M. L., Langre E. de, and Biolley F. (2004). Coupling of structure and wake oscillators in vortex-induced vibrations. *Journal of Fluids and Structures*, 19, 123-140.

[7] Farshidianfar A., Zanganeh H. (2010). A modified wake oscillator model for vortex-induced vibration of circular cylinder for a wide range of mass-damping ratio. *Journal of Fluids and Structures*, 26, 430-441.

[8] Gabbai R.D., Benaroya H. (2005). An overview of modeling and experiments of vortex-induced vibration of circular cylinders. *Journal of Sound and Vibration* 282, 575-616.

[9] Hartlen R.T., Currie I.G. (1970). Lift-oscillator model of vortex-induced vibration. *Journal of the Engineering Mechanics Division EM5*, 577-591.

[10] Iwan W.D., Blevins R.D. (1974). A model for vortex induced oscillation of structures. *Journal of Applied Mechanics* 41(3), 581-586.

[11] Khalak A., Williamson C.H.K. (1999). Motions, forces and mode transitions in vortex-induced vibrations at low mass-damping. Journal *of Fluids and Structures* 13, 813-851.

[12] Krenk S., Nielsen S. R. K. (1999) Energy balanced double oscillator model for vortex-induced vibrations. *ASCE Journal of Engineering Mechanics*, 125(3), 263-271.

[13] Kumar, Ravi T.R. Personal Communication. 2010-2011.

[14] Lin L., Ling G., Wu, Y., Zeng X. (2009). Nonlinear fluid damping in structure-wake oscillators in modeling vortex-induced vibrations. *Journal of Hydrodynamics*, 21(1), 1-11.

[15] Masud, A., Calderer, R. (2009). A variational multiscale stabilized formulation for the Incompressible navier-stokes equations. *Computational Mechanics* 44, 145–160, 10.1007/s00466-008-0362-3.

[16] Ogink R.H.M., Metrikine A.V. (2008). A wake oscillator with frequency dependent tuning coefficients for the modeling of VIV. *Proceedings of the ASME 27th International Conference on Offshore Mechanics and Arctic Engineering* Jun15-20, 2008, Estoril, Portugal.

[17] Ogink R.H.M., Metrikine A.V. (2010). A wake oscillator with frequency dependent coupling for the modeling of vortex-induced vibration. *Journal of Sound and Vibration* 329, 5452-5473.

[18] Skop R.A., Griffin O.M. (1973). A model for the vortex-excited resonant response of bluff cylinders. *Journal of Sound and Vibration*, 27(2), 225-233.

[19] Skop R.A. (1974). On modeling vortex-excited oscillations. *NRL Memorandum Report 2927*

[20] Skop R.A., Balasubramanian S. (1997). A new twist on an old model for vortex-excited vibrations. *Journal of Fluids and Structures* 11, 395-412.

[21] White, Frank M. (2006). *Viscous Fluid Flow.* 3rd ed. New York, NY: McGraw-Hill Higher Education, 8-12. Print.